Part II

Convection in Earth's mantle

Outline

Plate tectonics

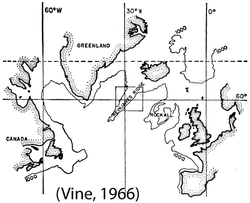

(Vine, 1966)

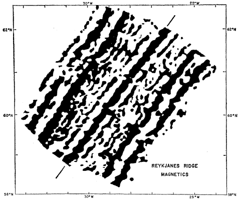

Plate tectonics

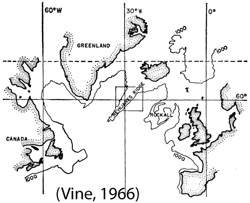

(Vine, 1966)

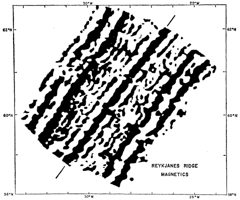

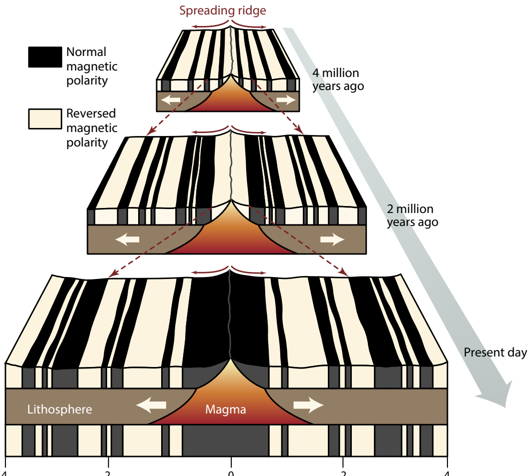

(Tivey, 2004)

Plate tectonics

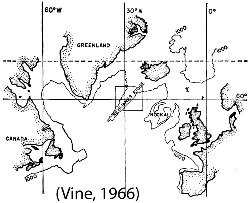

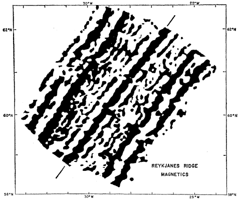

(Vine, 1966)

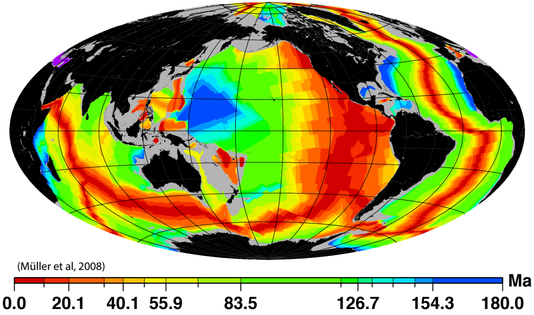

(Müller et al, 2008)

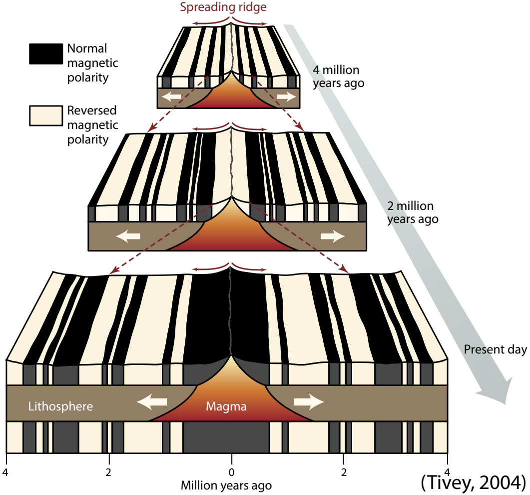

(Tivey, 2004)

Thermal structure of the oceanic lithosphere

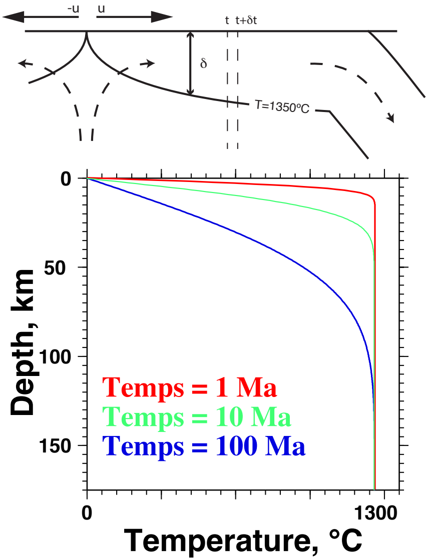

- A cold front propagates downward in the mantle as the plate moves away from the ridge
- The temperature follows the solution for the cooling of an infinite half–space:

$$T(z) = T_M \,\mathrm{erf}\, \frac{z}{2\sqrt{\kappa t}}$$
$$= \frac{2\,T_M}{\sqrt{\pi}} \int_0^{z/2\sqrt{\kappa t}} e^{-x^2}\, dx$$

- The heat flux decrease with the age of the plate as

$$q(t) = \frac{kT_M}{\sqrt{\pi \kappa t}} = C_Q t^{-1/2}$$

- C_Q can be determined by fitting the observed flux in well sedimented areas.

Heat flow data from well–sedimented areas
Lister et al. (1990)

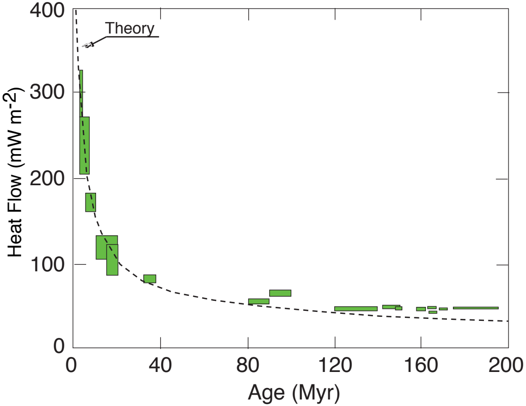

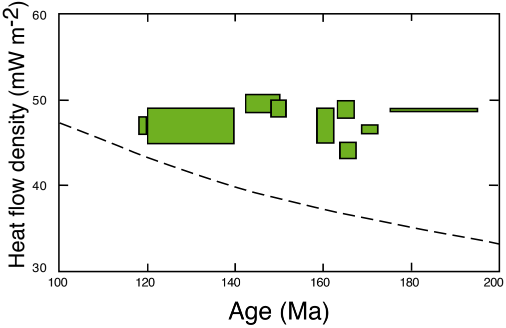

(Lister et al., 1990)

- $q = C_Q/\sqrt{t}$ valid for t up to 80 Myr with $475 \leq C_Q \leq 500 \Rightarrow T_M = 1300\,^\circ$C.
- Deviations for ages > 80 Myr: small–scale convection under the lithosphere.

Young oceans
Davis et al. (1999)

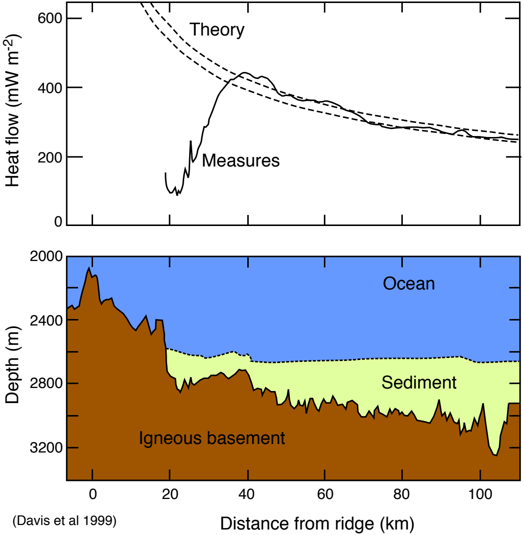

(Davis et al 1999)

- Impressive match between theory and observations when the sedimentary cover is sufficient
  - to properly measure the heat flow
  - and limit hydrothermal activity.

Another piece of evidence: Topography

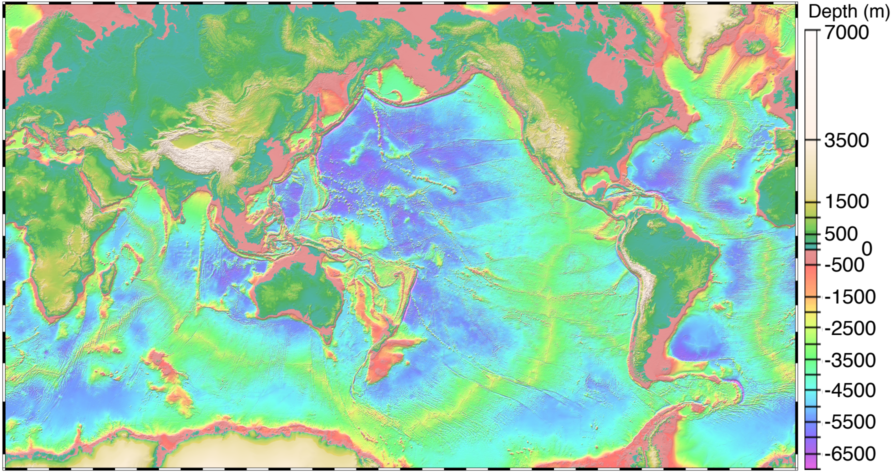

(Smith and Sandwell, 1997)

Isostatic theory for the ocean topography

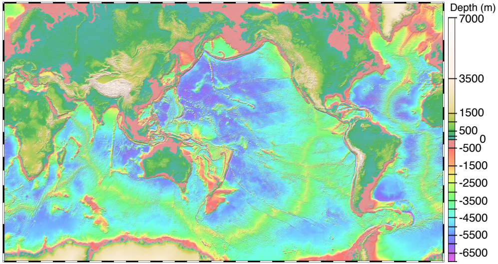

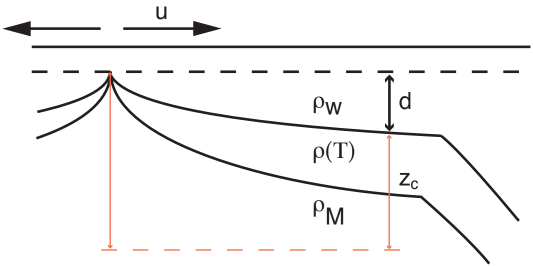

Thermal contraction ⇒ subsidence of the seafloor with age.

$$z = \frac{\rho_M}{\rho_M - \rho_w} 2\alpha T_M \sqrt{\frac{\kappa t}{\pi}}$$

Test of the theory

Carlson and Johnson (1994)

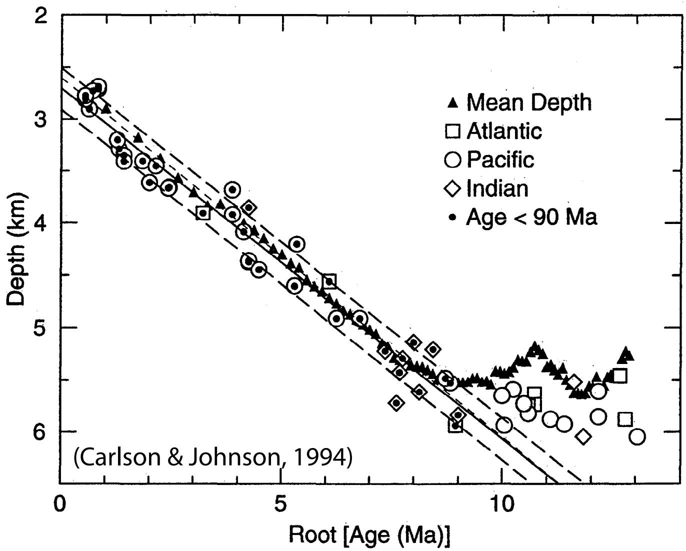

Oceanic heat flow

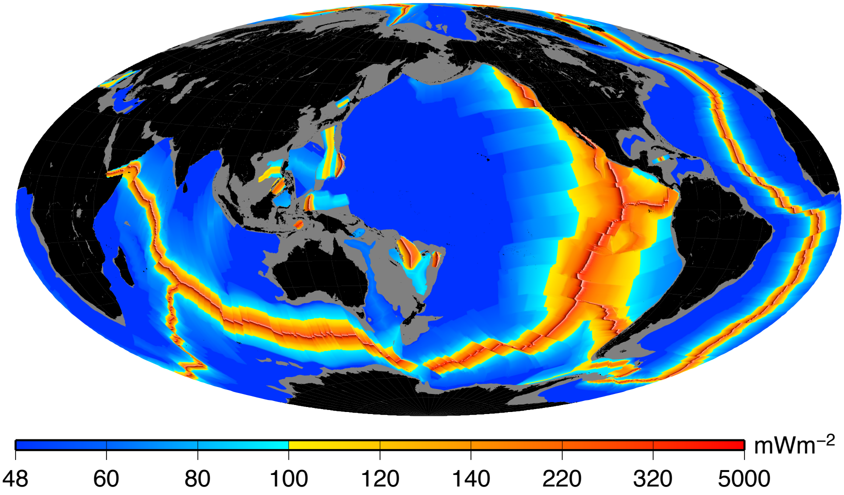

- Use seafloor age map.
- Apply $q = C_Q/\sqrt{t}$
- Total: 29 ± 1 TW from normal oceans.
- Add 2 TW to 4 TW from hotspots.

Total heat flow at Earth's surface
Jaupart et al. (2015)

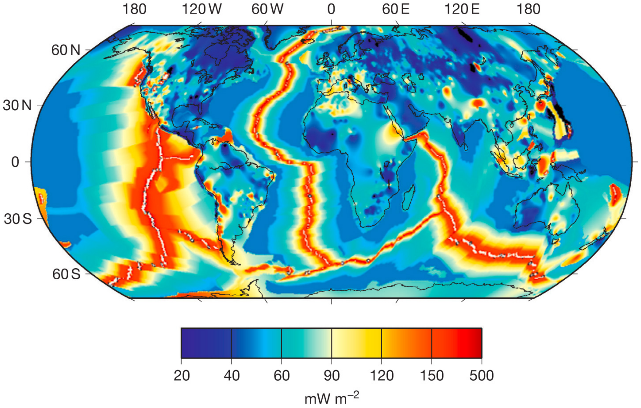

- The total heat loss of the Earth is $\simeq$ 46 TW
- The average heat flow density is 90 mWm^{-2}, corresponding to a mean temperature gradient of 30 Kkm^{-1}. The gradient must level off to match a central temperature $T_c \sim$ 6000 K.

$\Rightarrow$ A more efficient heat transfer mechanism is necessary at depth.

Advection in the mantle: order of magnitude

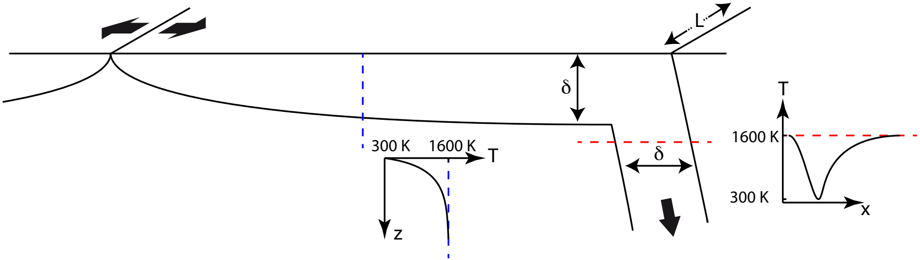

- Subduction :
  - length $L = 48\,800$ km.
  - mean temperature anomaly $\delta T \sim 600$ K.
  - typical velocity $w \sim 10$ cm/yr
  - thickness $\delta x \sim 100$ km

  $\Rightarrow$ Total advective flux: $Q = \delta x L \rho C_p w \delta T \simeq 30$ TW
- Plumes: very small surface $\Rightarrow$ 2 TW

Computation of the predicted temperature variations induced in the mantle by injection of cold plates in the past ~ 180 Ma (Ricard et al., 1993) and comparison with tomographic models.

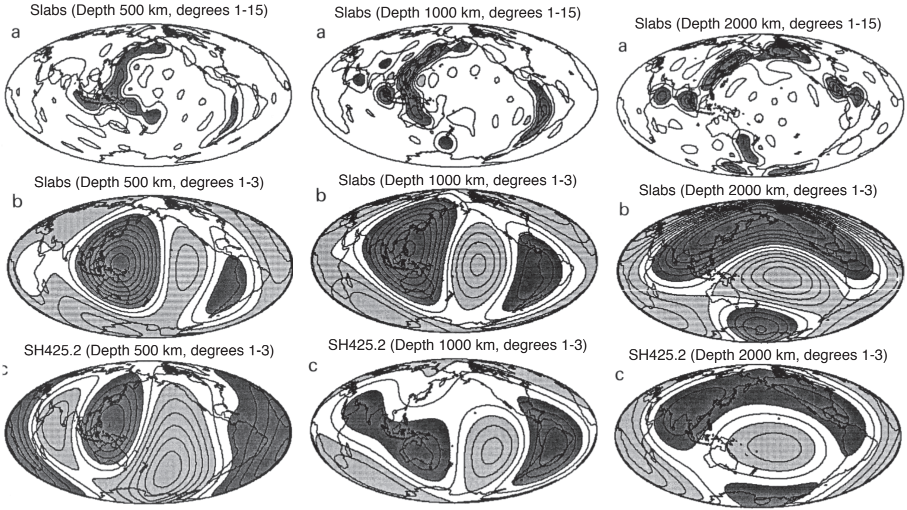

(Ricard et al, 1993) (Ricard et al, 1993) (Ricard et al, 1993)

Computation of the predicted temperature variations induced in the mantle by injection of cold plates in the past ~ 180 Ma (Ricard et al., 1993) and comparison with tomographic models.

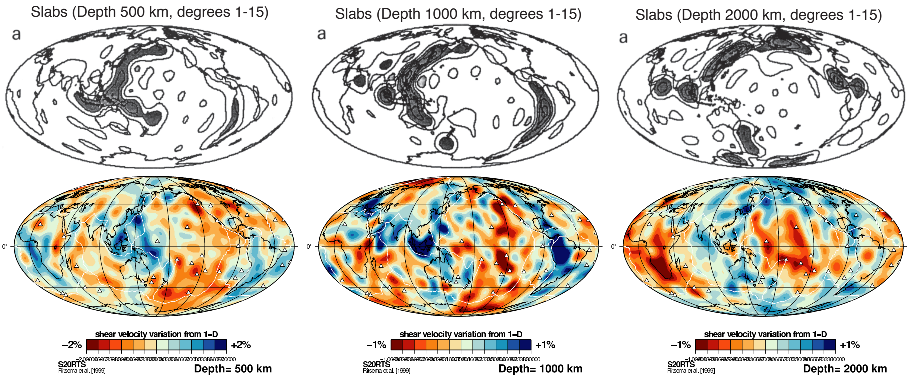

Seismic tomography: Ritsema et al. (1999).

Some peculiarities of mantle convection

- Internally heated by radioactivity and secularly cooled.
- Spherical shell geometry.
- Temperature–dependent viscosity and even complex rheology. Necessary to explain plate-tectonics.
- Depth– and temperature–dependence of all physical parameters
  $\Rightarrow$ compressible models may be necessary
- Variations of composition at various scales.
- Effects of continents.
- Two–phase flow (not covered in details).

Outline

Earth heat budget (Jaupart et al., 2015):

- Total heat flow at the surface of the solid Earth is $\simeq 46\,\mathrm{TW}$.
- Total radiogenic heat production is $\simeq 20\,\mathrm{TW}$.

$\Rightarrow$ Important to consider internal heating.

- And also secular cooling, which is equivalent (Krishnamurti, 1968): Consider that the average temperature $\langle T \rangle$ decreases with time on a long timescale t_a compared to the dynamical one t_c and $T = \langle T \rangle + T'$. Time derivative of temperature can be separated in slow and fast contribution so

$$\rho C \left(\frac{\partial T'}{\partial t_c} + \boldsymbol{u} \cdot \boldsymbol{\nabla} T' \right) = k \boldsymbol{\nabla}^2 T' + \underbrace{\rho h - \rho C \frac{\mathrm{d} \langle T \rangle}{\mathrm{d} t_a}}_{\text{effective internal heating}}$$

- With the same choice of scaling as before, the dimensionless equation is

$$\frac{\partial T}{\partial t} + \boldsymbol{u} \cdot \boldsymbol{\nabla} T = \boldsymbol{\nabla}^2 T + H \text{ with } H = \frac{\rho h d^2}{k \Delta T}$$

- At infinite *Pr*, two dimensionless parameters: *Ra* and H or *Ra* and $Ra_h = Ra H$.

Planform for internally heated convection

- The dynamics is dominated by downwelling cold plumes.
- Hot plumes are often triggered by the spreading of cold matter on the bottom boundary layer.
- Heat transfer is dominated by advection associated with cold currents.

Balance between conduction at the surface and advection at depth

- Heat balance between the surface and depth z :

$$q_0 \equiv \left(k\frac{\partial T}{\partial z}\right)_0 = \underbrace{k\left(\frac{\partial T}{\partial z}\right)_z}_{Conduction} + \underbrace{\rho C_p \overline{w\delta T}}_{Advection} + \underbrace{\rho H z}_{Radioactivity}$$

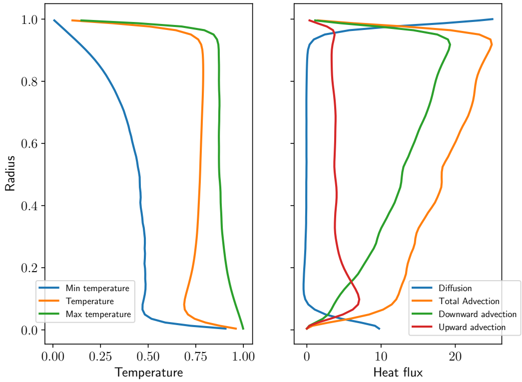

- More buoyancy available from cold than hot anomalies.
- Advection dominated by downwelling of upwelling currents.
- Energy balance $\Rightarrow$ advection increases linearly with height.

Temperature profiles and heat flux scaling with internal heating
Sotin and Labrosse (1999)

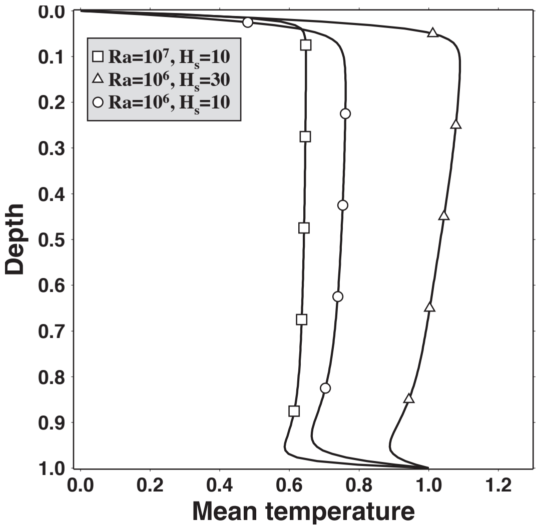

- Two dimensionless parameters *Ra* et H.
- Surface heat flux controlled by the stability of the boundary layer. Local Rayleigh number:

$$Ra_\delta = \frac{\Delta T_s}{\Delta T}\frac{\delta^3}{d^3} Ra = R_c$$

$$\Rightarrow q = \frac{k\Delta T_s}{\delta}$$

$$= \frac{k\Delta T}{d}\left(\frac{Ra}{R_c}\right)^{1/3}\left(\frac{\Delta T_s}{\Delta T}\right)^{4/3}$$

Average temperature
Sotin and Labrosse (1999)

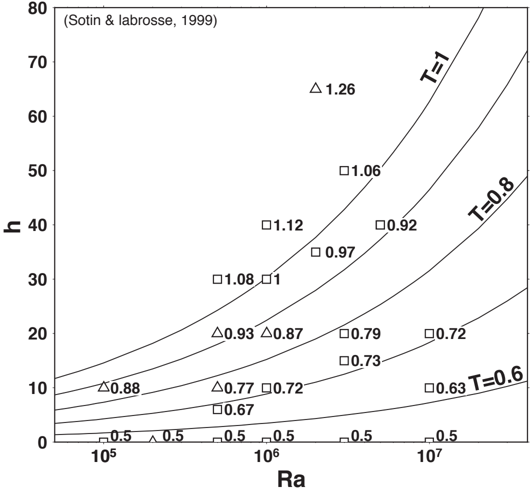

Two contributions:

- Symmetrical case (no internal heating): $\langle T \rangle = 1/2$.
- Additional term from internal heating. In the limit of zero bottom heat flux,

$$H = q \sim Ra^{1/3} \langle T \rangle^{4/3} \Rightarrow \langle T \rangle \sim \frac{H^{3/4}}{Ra^{1/4}}$$

- Total:

$$\langle T \rangle = \frac{1}{2} + \frac{H^{3/4}}{Ra^{1/4}}$$

Convection driven by internal heating only

Parmentier and Sotin (2000)

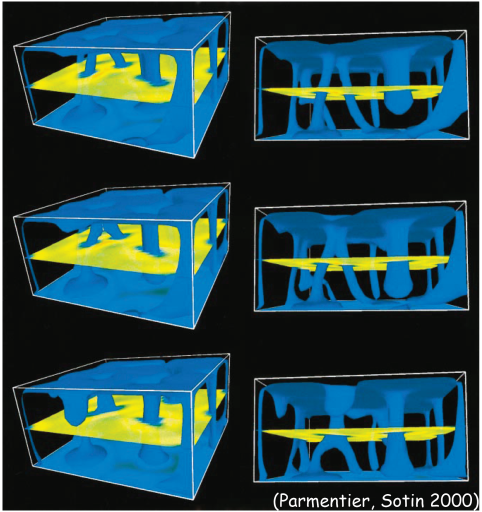

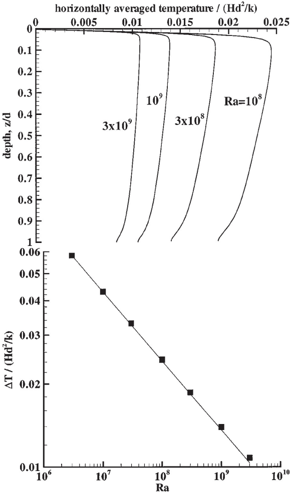

- Internal heating *Ra*

$$Ra_h = \frac{\alpha g \rho h d^5}{k \kappa \nu}$$

- Energy balance:

$$q = \rho h d = k \frac{\Delta T}{\delta}$$

- BL stability:

$$Ra_\delta = Ra_h \left(\frac{\delta}{d}\right)^4 = R_c$$

-

$$\Delta T = \frac{\rho h d^2}{k} Ra_h^{-1/4}$$

Outline

Toroidal-poloidal decomposition of surface velocity
Ribe (2018)

- The divergence–free velocity field can be written as

$$\boldsymbol{u} = \underbrace{\boldsymbol{\nabla} \times r\boldsymbol{e}_r \times \boldsymbol{\nabla}\mathcal{P}}_{Poloidal} + \underbrace{r\boldsymbol{e}_r \times \boldsymbol{\nabla}\mathcal{T}}_{Toroidal} \tag{1}$$

$$= \boldsymbol{e}_\theta \left[-\frac{1}{r}\frac{\partial^2 r\mathcal{P}}{\partial r^1 \partial \theta^1} - \frac{1}{\sin\theta}\frac{\partial \mathcal{T}}{\partial \phi} \right] + \boldsymbol{e}_\phi \left[-\frac{1}{r\sin\theta}\frac{\partial^2 r\mathcal{P}}{\partial r^1 \partial \phi^1} + \frac{\partial \mathcal{T}}{\partial \theta} \right] + \frac{\boldsymbol{e}_r}{r}\mathcal{B}^2\mathcal{P} \tag{2}$$

with

$$\mathcal{B}^2 = \frac{1}{\sin\theta}\frac{\partial}{\partial\theta}\sin\theta\frac{\partial}{\partial\theta} + \frac{1}{\sin^2\theta}\frac{\partial^2}{\partial\phi^2}$$

- For a constant viscosity fluid, apply $\nabla \times (r\boldsymbol{e}_r \times \nabla)$ and $r\boldsymbol{e}_r \times \nabla$ to the momentum equation:

$$\mathcal{B}^2\nabla^4\mathcal{P} = \frac{g}{\eta r}\mathcal{B}^2\Delta\rho; \quad \mathcal{B}^2\nabla^2\mathcal{T} = 0$$

- Internal loads can only create a poloidal flow (the same is true for $\eta(r)$).
- Also useful to define the horizontal divergence and the radial vorticity:

$$\nabla_h \cdot \boldsymbol{u} = -\mathcal{B}^2\left[\frac{1}{r^2}\frac{\partial r\mathcal{P}}{\partial r}\right]; \quad \boldsymbol{e}_r \cdot (\nabla \times \boldsymbol{u}) = \frac{\mathcal{B}^2\mathcal{T}}{r}$$

Toroidal-poloidal decomposition of surface velocity

Ribe (2018)

- The divergence–free velocity field can be written as

$$\boldsymbol{u} = \underbrace{\boldsymbol{\nabla} \times r\boldsymbol{e}_r \times \boldsymbol{\nabla}\mathcal{P}}_{Poloidal} + \underbrace{r\boldsymbol{e}_r \times \boldsymbol{\nabla}\mathcal{T}}_{Toroidal} \quad (1)$$

$$= \boldsymbol{e}_\theta \left[-\frac{1}{r}\frac{\partial^2 r\mathcal{P}}{\partial r^1 \partial\theta^1} - \frac{1}{\sin\theta}\frac{\partial\mathcal{T}}{\partial\phi} \right] + \boldsymbol{e}_\phi \left[-\frac{1}{r\sin\theta}\frac{\partial^2 r\mathcal{P}}{\partial r^1 \partial\phi^1} + \frac{\partial\mathcal{T}}{\partial\theta} \right] + \frac{\boldsymbol{e}_r}{r}\mathcal{B}^2\mathcal{P} \quad (2)$$

  with

$$\mathcal{B}^2 = \frac{1}{\sin\theta}\frac{\partial}{\partial\theta}\sin\theta\frac{\partial}{\partial\theta} + \frac{1}{\sin^2\theta}\frac{\partial^2}{\partial\phi^2}$$

- For a constant viscosity fluid, apply $\boldsymbol{\nabla} \times (r\boldsymbol{e}_r \times \boldsymbol{\nabla})$ and $r\boldsymbol{e}_r \times \boldsymbol{\nabla}$ to the momentum equation:

$$\mathcal{B}^2\nabla^4\mathcal{P} = \frac{g}{\eta r}\mathcal{B}^2\Delta\rho; \quad \mathcal{B}^2\nabla^2\mathcal{T} = 0$$

- Internal loads can only create a poloidal flow (the same is true for $\eta(r)$).
- Also useful to define the horizontal divergence and the radial vorticity:

$$\nabla_h \cdot \boldsymbol{u} = -\mathcal{B}^2\left[\frac{1}{r^2}\frac{\partial r\mathcal{P}}{\partial r}\right]; \quad \boldsymbol{e}_r \cdot (\boldsymbol{\nabla} \times \boldsymbol{u}) = \frac{\mathcal{B}^2\mathcal{T}}{r}$$

Toroidal-poloidal decomposition of surface velocity
Ribe (2018)

- The divergence–free velocity field can be written as

$$\boldsymbol{u} = \underbrace{\boldsymbol{\nabla} \times r\boldsymbol{e}_r \times \boldsymbol{\nabla}\mathcal{P}}_{Poloidal} + \underbrace{r\boldsymbol{e}_r \times \boldsymbol{\nabla}\mathcal{T}}_{Toroidal} \tag{1}$$

$$= \boldsymbol{e}_\theta \left[-\frac{1}{r}\frac{\partial^2 r\mathcal{P}}{\partial r^1 \partial\theta^1} - \frac{1}{\sin\theta}\frac{\partial\mathcal{T}}{\partial\phi} \right] + \boldsymbol{e}_\phi \left[-\frac{1}{r\sin\theta}\frac{\partial^2 r\mathcal{P}}{\partial r^1 \partial\phi^1} + \frac{\partial\mathcal{T}}{\partial\theta} \right] + \frac{\boldsymbol{e}_r}{r}\mathcal{B}^2\mathcal{P} \tag{2}$$

with

$$\mathcal{B}^2 = \frac{1}{\sin\theta}\frac{\partial}{\partial\theta}\sin\theta\frac{\partial}{\partial\theta} + \frac{1}{\sin^2\theta}\frac{\partial^2}{\partial\phi^2}$$

- For a constant viscosity fluid, apply $\boldsymbol{\nabla} \times (r\boldsymbol{e}_r \times \boldsymbol{\nabla})$ and $r\boldsymbol{e}_r \times \boldsymbol{\nabla}$ to the momentum equation:

$$\mathcal{B}^2\nabla^4\mathcal{P} = \frac{g}{\eta r}\mathcal{B}^2\Delta\rho; \quad \mathcal{B}^2\nabla^2\mathcal{T} = 0$$

- Internal loads can only create a poloidal flow (the same is true for $\eta(r)$).
- Also useful to define the horizontal divergence and the radial vorticity:

$$\nabla_h \cdot \boldsymbol{u} = -\mathcal{B}^2\left[\frac{1}{r^2}\frac{\partial r\mathcal{P}}{\partial r}\right]; \quad \boldsymbol{e}_r \cdot (\boldsymbol{\nabla} \times \boldsymbol{u}) = \frac{\mathcal{B}^2\mathcal{T}}{r}$$

Toroidal-poloidal decomposition of surface velocity
Ribe (2018)

- The divergence–free velocity field can be written as

$$\boldsymbol{u} = \underbrace{\boldsymbol{\nabla} \times r\boldsymbol{e}_r \times \boldsymbol{\nabla}\mathcal{P}}_{Poloidal} + \underbrace{r\boldsymbol{e}_r \times \boldsymbol{\nabla}\mathcal{T}}_{Toroidal} \tag{1}$$

$$= \boldsymbol{e}_\theta \left[-\frac{1}{r} \frac{\partial^2 r\mathcal{P}}{\partial r^1 \partial \theta^1} - \frac{1}{\sin\theta} \frac{\partial \mathcal{T}}{\partial \phi} \right] + \boldsymbol{e}_\phi \left[-\frac{1}{r\sin\theta} \frac{\partial^2 r\mathcal{P}}{\partial r^1 \partial \phi^1} + \frac{\partial \mathcal{T}}{\partial \theta} \right] + \frac{\boldsymbol{e}_r}{r} \mathcal{B}^2 \mathcal{P} \tag{2}$$

with

$$\mathcal{B}^2 = \frac{1}{\sin\theta} \frac{\partial}{\partial\theta} \sin\theta \frac{\partial}{\partial\theta} + \frac{1}{\sin^2\theta} \frac{\partial^2}{\partial\phi^2}$$

- For a constant viscosity fluid, apply $\boldsymbol{\nabla} \times (r\boldsymbol{e}_r \times \boldsymbol{\nabla})$ and $r\boldsymbol{e}_r \times \boldsymbol{\nabla}$ to the momentum equation:

$$\mathcal{B}^2 \nabla^4 \mathcal{P} = \frac{g}{\eta r} \mathcal{B}^2 \Delta\rho; \quad \mathcal{B}^2 \nabla^2 \mathcal{T} = 0$$

- Internal loads can only create a poloidal flow (the same is true for $\eta(r)$).
- Also useful to define the horizontal divergence and the radial vorticity:

$$\boldsymbol{\nabla}_h \cdot \boldsymbol{u} = -\mathcal{B}^2 \left[\frac{1}{r^2} \frac{\partial r\mathcal{P}}{\partial r} \right]; \quad \boldsymbol{e}_r \cdot (\boldsymbol{\nabla} \times \boldsymbol{u}) = \frac{\mathcal{B}^2 \mathcal{T}}{r}$$

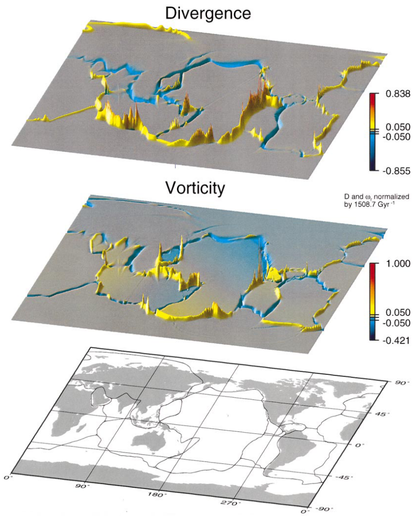

Figure 7. Same as Fig. 6 but with horizontal divergence and radial vorticity calculated directly from the velocity field of the SEISMAR plate model.
(Dumoulin et al, 1998)

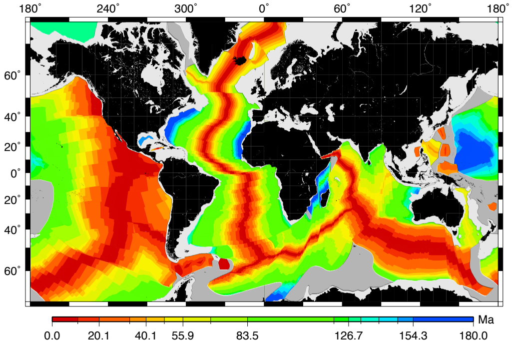

- Seafloor ages
  $\rightarrow$ plate velocities.
- Toroidal flow $\Rightarrow$ Lateral variations of viscosity are necessary to generate it.

(Dumoulin et al., 1998)

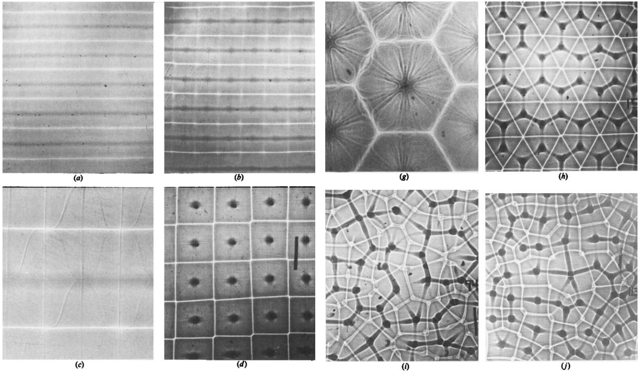

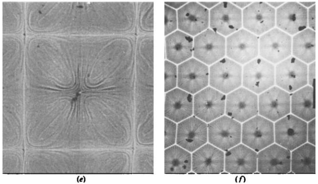

White (1988):
a : rolls
b, c : bimodal
d, e : square
f, g : hexagones
h : triangles
i, j : spoke

- First effect: breaking the symmetry between up- and downwelling currents.

⇒ Allows different flow geometries.

- These experiments: modest variations of viscosity.

Large temperature-dependence of viscosity I

$\mathrm{Ra} = 10^8$

$\eta_{max}/\eta_{min} = 10^6$

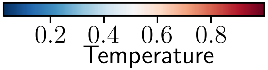

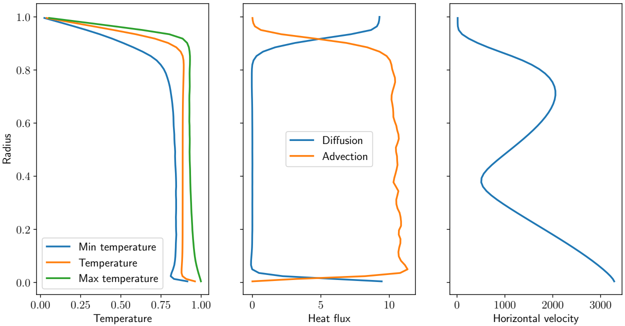

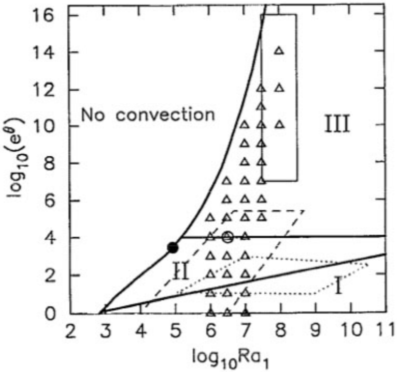

(Moresi and Solomatov, 1995) identified 3 regimes:

- I: small viscosity contrast regime
- II: transitional regime
- III: stagnant lid regime

Transient experiments
Davaille and Jaupart (1993, 1994)

- A tank filled with golden syrup with the upper boundary maintained at a low temperature.
- Explains very well the onset of small–scale convection below the oceanic lithophere.

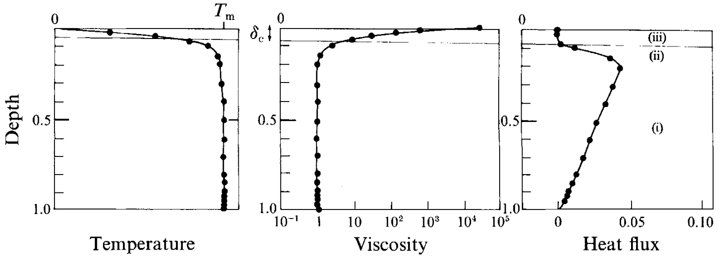

FIGURE 5. Vertical profiles of horizontally averaged temperature, viscosity and convective heat flux for fully developed convection in experiment 4.41. Viscosity and heat flux have been made dimensionless using viscosity at the interior temperature and the local heat flux scale Q_b (equation (12)) respectively. The fluid layer can be divided in (i) the well-mixed interior, (ii) the unstable part of the thermal boundary layer and (iii) a stagnant lid. (Davaille & Jaupart, 1993)

Transient experiments
Davaille and Jaupart (1993, 1994)

- A tank filled with golden syrup with the upper boundary maintained at a low temperature.
- Explains very well the onset of small–scale convection below the oceanic lithophere.

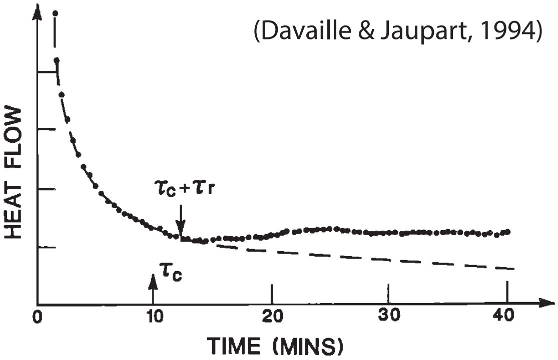

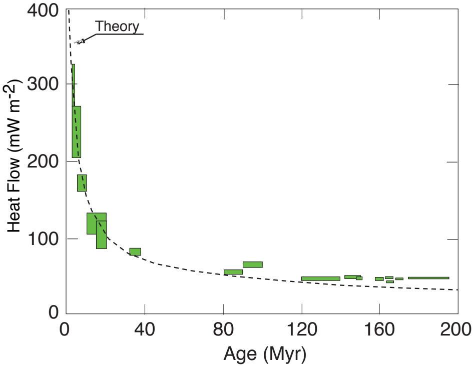

Strain localisation by pseudo-plasticity
Tackley (2000)

- Temperature dependence of viscosity allows to rigidify plates:

$$\eta(T) = \eta_0 \, e^{E/RT}$$

- A yield stress σ_y is introduced to saturate stress once a critical deformation is reached:

$$\eta_{\mathit{eff}} = \min\left[\eta(T), \frac{\sigma_y}{2\dot{\varepsilon}}\right]$$

with $\dot{\varepsilon} = \sqrt{\dot{\varepsilon}_{ij}\dot{\varepsilon}_{ij}}$

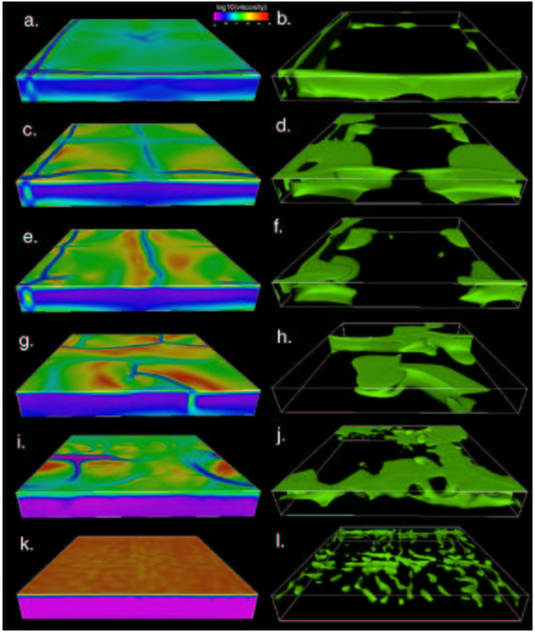

Tackley (2000)

- Left: effective viscosity
- Right: temperature
- Yield stress increases from top to bottom, $34\ \mathrm{MPa}$ to $340\ \mathrm{MPa}$

Example dynamics in 2D

- Converging zones (subduction) attract each other $\rightarrow$ merging.
- Diverging zones are passive and adjust to the position of subductions $\rightarrow$ jump.
- Very large fluctuations of temperature and heat fluxes.

Motion on plate boundaries

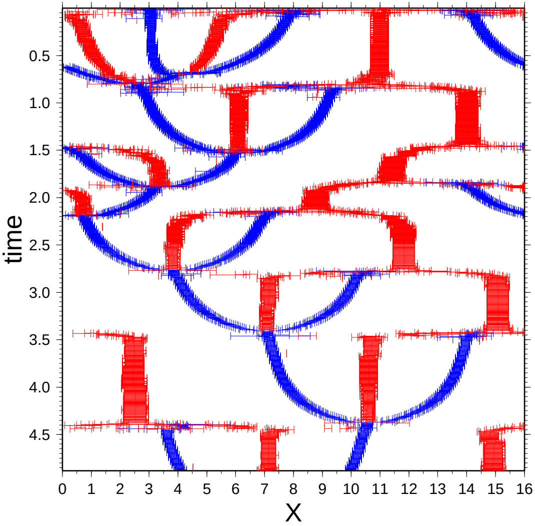

- Converging zones (subduction) attract each other → merging.
- Diverging zones are passive and adjust to the position of subductions → jump.
- Very large fluctuations of temperature and heat fluxes.

Heat flow and plate size

Grigné et al. (2005)

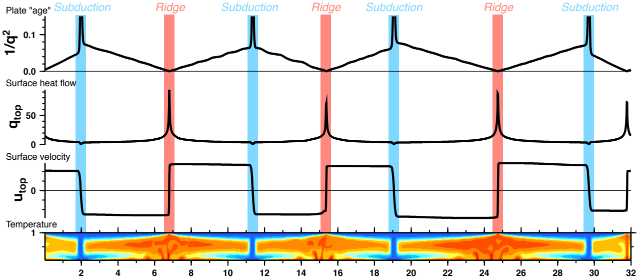

(Grigné et al, 2005 ; Labrosse & Jaupart, 2007)

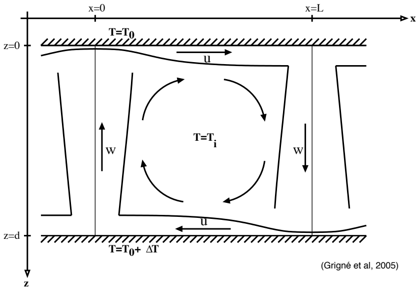

(Grigné et al, 2005)

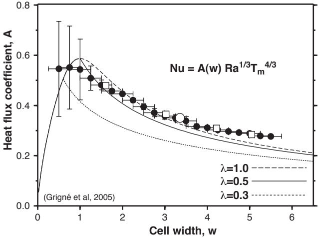

(Grigné et al, 2005)

- Loop model: balance between buoyancy and viscous resistance

$$\Rightarrow q_{top} = C(L) Ra_m^{1/3} T_m^{4/3}$$

$\Rightarrow$ classical scaling supported by convection models with self-consistent plate tectonics (pseudo-plastic rheology).

Issues and potential solutions

A rather simple rheology (pseudo-plastic) allows to obtain a dynamics mimicking some aspects of plate tectonics. But...

- How does it relate to the actual rheology of rocks? In particular the yield stress necessary to get plate-like behaviour is generally smaller than that measured in laboratory.
- On Earth, old deformation structures often get reactivated $\rightarrow$ the rheology is history dependent. A damage theory is needed.
  - Bercovici and Ricard (2014): grain-size dependence in a multi-mineral rock with Zener pinning.
  - Anisotropic viscosity with lattice preferred orientation (Pouilloux et al., 2007)? Theory and models still needed for that.

Outline

The isentropic temperature gradient

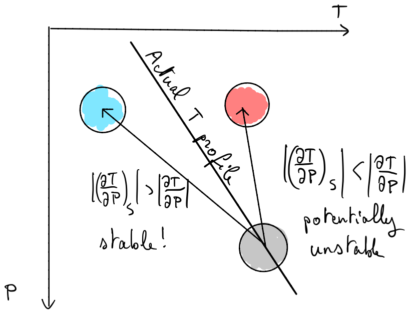

- Compression $\Rightarrow$ increase of temperature $\rightarrow$ useless part of the temperature gradient.
- Isentropic gradient ($\sim$ adiabatic)

$$\left(\frac{\partial T}{\partial P}\right)_s = \frac{\alpha T}{\rho C_p} \Rightarrow \frac{\partial T}{\partial r} = -\frac{\alpha g T}{C_p}$$

- Solution to subtract from the total ΔT:

$$T(r) = T_0 \exp\left(-\int_{CMB}^{r} \frac{\alpha g}{C_p}\, dr\right)$$

- T_0 : “foot of the adiabat”.
- Jeffreys (1930) showed that the criterion for Rayleigh–Bénard instability in a “weakly compressible” fluid is the same as that derived by Rayleigh (1916) provided the temperature difference is taken as that in excess of the isentropic one.

Equations for compressible convection
Curbelo et al. (2019)

$$\frac{\partial \rho}{\partial t} + \boldsymbol{\nabla} \cdot (\rho \mathbf{v}) = 0, \tag{3}$$

$$\mathbf{0} = -\boldsymbol{\nabla} P + \rho \mathbf{g} + \boldsymbol{\nabla} \cdot \tau, \tag{4}$$

$$\rho T \left[\frac{\partial s}{\partial t} + \mathbf{v} \cdot \boldsymbol{\nabla} s \right] = \dot{\varepsilon} : \tau + \boldsymbol{\nabla} \cdot (k \boldsymbol{\nabla} T), \tag{5}$$

$$T = T(\rho, s), \qquad P = P(\rho, s), \tag{6}$$

with the deformation rate tensor $\dot{\varepsilon}$ and stress tensor τ:

$$\dot{\varepsilon}_{ij} = \frac{1}{2} (\partial_j v_i + \partial_i v_j), \qquad \tau_{ij} = \eta \left(\partial_j v_i + \partial_i v_j - \frac{2}{3} \delta_{ij} \boldsymbol{\nabla} \cdot \mathbf{v} \right), \tag{7}$$

The equations are rendered dimensionless using

$$t \to \rho_0 c_{p0} d^2/k;\ (x, z) \to d;\ (u_x, u_z) \to k/(\rho_0 c_{p0} d);\ T \to T_0;\ P \to \rho_0 c_{p0} T_0;$$
$$s \to c_{p0};\ \dot{\varepsilon}_{ij} \to k/(\rho_0 c_{p0} d^2);\ \tau \to k\eta/(\rho_0 c_{p0} d^2).$$

Dimensionless equations for compressible convection
Curbelo et al. (2019)

$$\frac{\partial \rho}{\partial t} + \boldsymbol{\nabla} \cdot (\rho \mathbf{v}) = 0, \tag{8}$$

$$\mathbf{0} = -\frac{R\hat{\alpha}}{\mathcal{D}} \boldsymbol{\nabla} P - R\rho \mathbf{e}_z + \boldsymbol{\nabla} \cdot \tau, \tag{9}$$

$$\rho T \left[\frac{\partial s}{\partial t} + \mathbf{v} \cdot \boldsymbol{\nabla} s\right] = \frac{\mathcal{D}}{R\hat{\alpha}} \dot{\varepsilon} : \tau + \nabla^2 T, \tag{10}$$

$$T = T(\rho, s), \qquad P = P(\rho, s), \tag{11}$$

$$\dot{\varepsilon}_{ij} = \frac{1}{2}\left(\partial_j v_i + \partial_i v_j\right), \qquad \tau_{ij} = \partial_j v_i + \partial_i v_j - \frac{2}{3}\delta_{ij} \boldsymbol{\nabla} \cdot \mathbf{v}, \tag{12}$$

Dimensionless numbers:

$R = \frac{\rho_0^2 c_{p0}\, g d^3}{k\eta}$ $\qquad r = T_{bot}/T_{top}$

$\hat{\alpha} = \alpha_0 T_0$ $\qquad \epsilon = \Delta T_{sa}/\Delta T_a$

$\mathcal{D} = \frac{\alpha_0\, g d}{c_{p0}}$ $\qquad Ra_{sa} = R\hat{\alpha}\delta T_{sa} = R\hat{\alpha}\epsilon\delta T_a = R\hat{\alpha}\frac{\epsilon}{1+\epsilon}\delta T$

The Boussinesq approximation is obtained by applying $\lim\limits_{r\to 1} \lim\limits_{\mathcal{D}\to 0}$.

Usual approximations

- The anelastic approximation, AA, is a linear development around the isentropic reference.
- The anelastic liquid approximation assumes, in addition, $\hat{\alpha} = \alpha T_0 \ll 1$.
- The extended Boussinesq approximation just considers dissipation on the right–hand–sides of the energy equation.
- The truncated anelastic liquid approximation neglects the pressure effect on buoyancy. It is not self–consistent (Leng and Zhong, 2008) as it does not satisfy the global balance between dissipation and the total work of the buoyancy force.

Comparison of the solutions
Perfect gas calculations (Curbelo et al., 2019)

$Ra_{sa} = 2 \times 10^4$ $\qquad$ $Ra_{sa} = 4 \times 10^4$

Full compressible

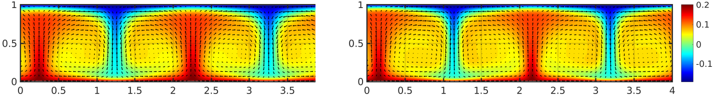

Anelastic Aproximation

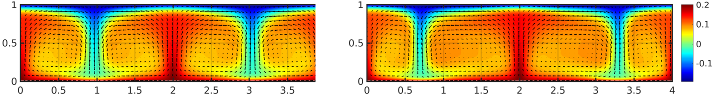

Anelastic liquid approximation

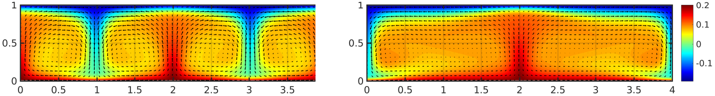

Comparison of average temperature profiles

Perfect gas calculations (Curbelo et al., 2019)

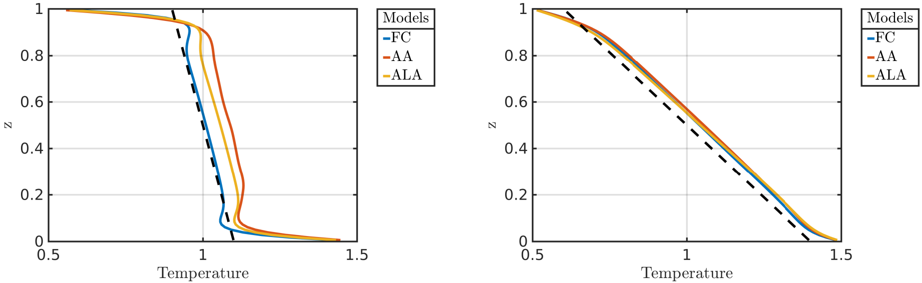

$Ra_{sa} = 320000$, $\gamma = 1.4$, $r = 3$, $\mathcal{D} = 0.2$ $(\epsilon = 4)$ on the left-hand side and $\mathcal{D} = 0.8$ $(\epsilon = 0.25)$ on the right-hand side (reference adiabatic profile shown in dashed line).

- All approximations converge when the super-isentropic temperature difference is small compared to the isentropic temperature difference $(\epsilon \ll 1)$.
- When ϵ is not too small, the temperature profile is qualitatively similar to the one obtained with the Boussinesq approximation with the addition of the isentropic profile.
- Earth's mantle: $\epsilon \sim 0.6$ and $\mathcal{D} \sim 0.5$.
- Earth's core: $\epsilon \sim 10^{-7}$ and $\mathcal{D} \sim 0.5$.

Outline

Compositional variations in the mantle and fluid dynamics

- Upper mantle: direct observations of strong compositional variations from the largest scale (continents and oceans) to the smallest (different minerals in a rock).
- Deep mantle: evidence come from geochemistry and geophysics (mostly seismology).
- Two types of compositional variations:
  - trace elements do not act on density but can play a role on radiogenic heating (^{235}U, ^{238}U, ^{232}Th, ^{40}K).
  - major elements, or oxydes (i.e. FeO and MgO), act on density and most physical parameters, like viscosity.
- In the fluid dynamics of mantle convection: add a new parameter, the buoyancy number,

$$B = \frac{\Delta \rho_\chi}{\rho_0 \alpha \Delta T} \text{ or } \mathit{Ra}_\chi = \mathit{Ra} B.$$

- The buoyancy term in the momentum equation is:

$$\mathit{Ra}(\theta + BC)$$

with C the dimensionless composition.

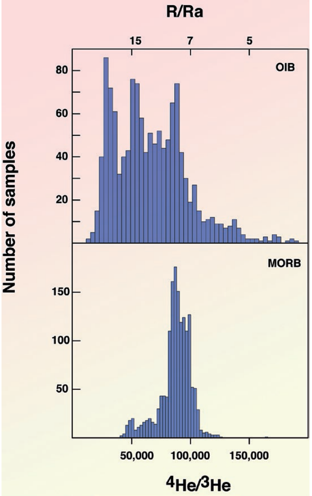

Figure 3.7 (Moreira, 2013)

- Mostly isotopic geochemistry, e.g. noble gas.
- Shows the need for a diversity of sources/history of mantle minerals.
- Example of noble gas: ^{3}He is primordial and ^{4}He is mostly radiogenic.
- MORB v.s. OIB: Existence of a deep undegassed mantle?

Conceptual models for the current snapshot

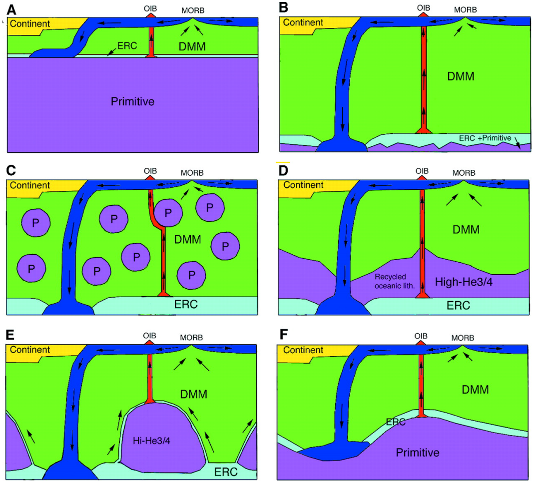

(Tackley, 2000)

Conceptual models for the current snapshot

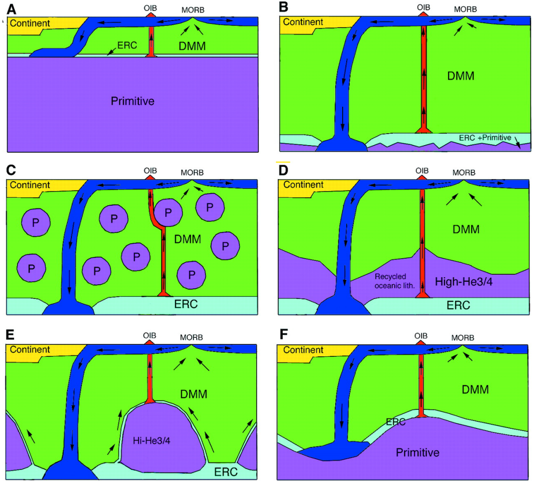

(Tackley, 2000)

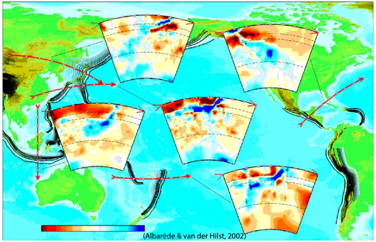

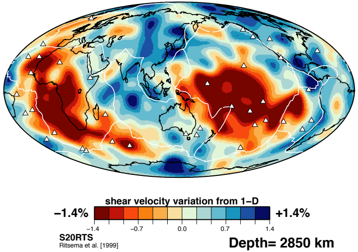

Dense partial melt pocket at the base of the mantle

- Large V_S anomalies in the lower mantle $\rightarrow$ thermal and chemical heterogeneity.
- ULVZs at the edges of dense thermo-chemical piles. Interpreted as pockets of dense partial melt.

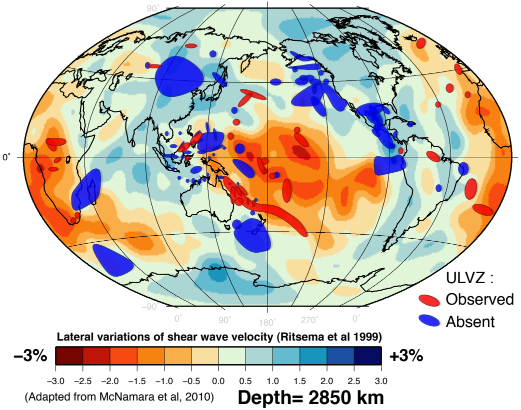

(Adapted from McNamara et al, 2010)

Various observations in Cartoon form
Hernlund & McNamara, ToG 2015

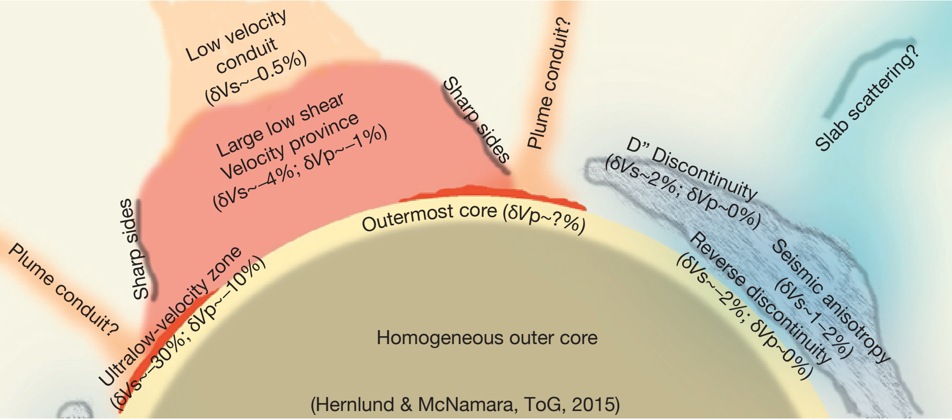

- Also: possible reflection from the top of LLSVPs (Schumacher, et al 2018)
- Simplest common ingredient to all these observations: Compositional variations.

The present snapshot and the long term evolution

- The present observations only constrain the current "snapshot" of the mantle.
- Different timescales of evolution: short (plate tectonics) and long (thermal evolution, regime changes?).
- Avoid the uniformitarian bias!

Stability of LLSVPs?

Burke & Torsvik (2004)

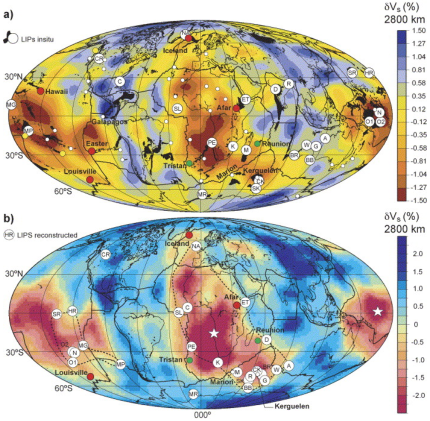

- (a) Current position of plumes (small circles) and Large Igneous Provinces (LIPs, large circles) at the present time over the seismic tomography model of Ritsema et al. (1999).
- (b) Reconstructed position of eruption sites of LIPs over the seismic tomography model SMEAN (Becker and Boschi, 2002).
- Position of large igneous provinces (LIPs) when erupted correlates with edges of LLSVPs.
- Suggests "long" (200Ma) term stability of these structures. Still compared to the age of the Earth!

LLSVs and ULVZs in models

McNamara, Garnero, Rost (2010)

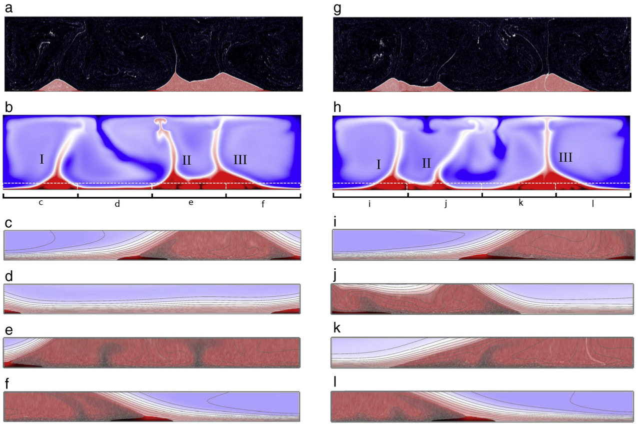

- Dense chemical piles move in response to plate and plume flow.
- ULVZs tend to be at the edges of piles because of viscous coupling with the surrounding mantle.
- But important transient effects $\rightarrow$ can be in the middle of a pile or isolated for some time.

Compositional layering of LLSVPs

Ballmer et al, 2016

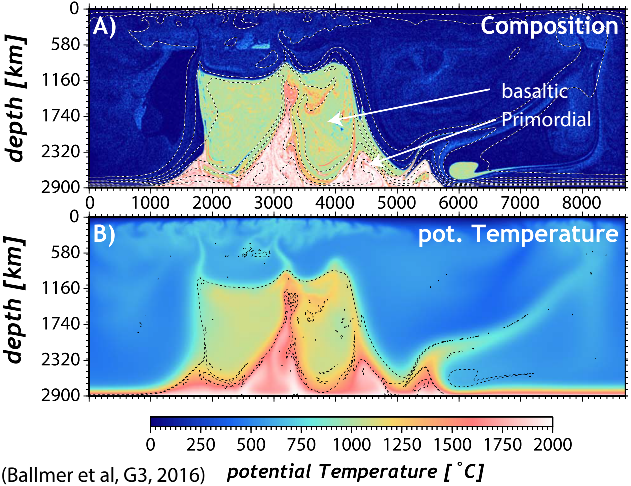

(Ballmer et al, G3, 2016)

bridgmanite-enriched ancient mantle structures (BEAMS)

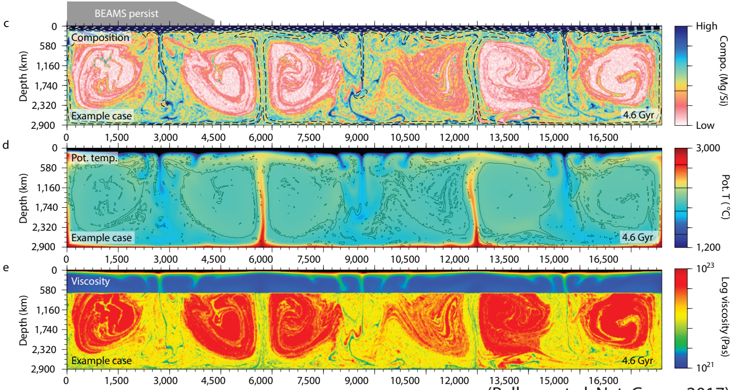

(Ballmer et al, Nat. Geosc. 2017)

- Non-linear viscosity variation depending on Si/Mg ratio.
- For $\eta_{max}/\eta_{min} > 100$ BEAMS forms.

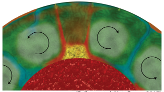

(Ballmer et al, Nat. Geosc. 2017)

Production of compositional anomalies

- Compositional anomalies are produced at the mineral scale.
- Large scale heterogeneities require entrainment and separation by solid mantle flow.
- Only a liquid phase permits longer distances separation. This can be
  - water $\rightarrow$ mostly a subduction/mantle corner process, possibly transition zone (Bercovici and Karato, 2003), not covered here.
  - liquid iron at the CMB $\rightarrow$ often considered limited by the large density contrast. Alternative have been proposed (Kanda and Stevenson, 2006; Otsuka and Karato, 2012) but have not been picked up in geodynamical models.
  - Liquid iron during core formation.
  - magma $\rightarrow$ fractional melting and freezing creates intermediate ($\sim$ km) scale heterogeneities at the surface (MORB) and possibly in the deep mantle (ULVZ), now and in the past (magma ocean).

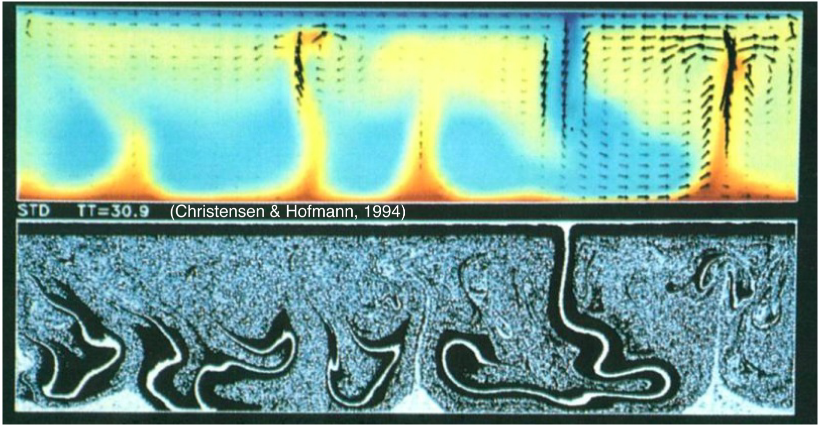

- Partial melting at ridges ⇒ production of compositional anomalies.
- Crust minerals become more dense than average mantle at high pressure ⇒ it could segregate into the deep mantle.

More sophisticated (recent) models
Nakagawa & Tackley (2008)

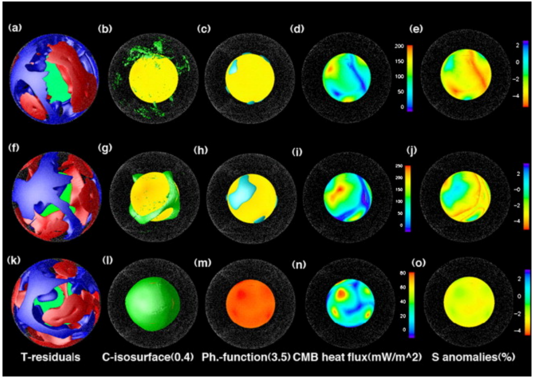

- Depending on the density contrast of MORB to normal mantle, it is entrained ($\delta\rho = 0$) or accumulate in ridge-like structures ($\delta\rho = 3.6\%$) or a continuous layer($\delta\rho = 17.3\%$).

Cycling oceanic crust through mantle reservoirs
Li et al. (2014)

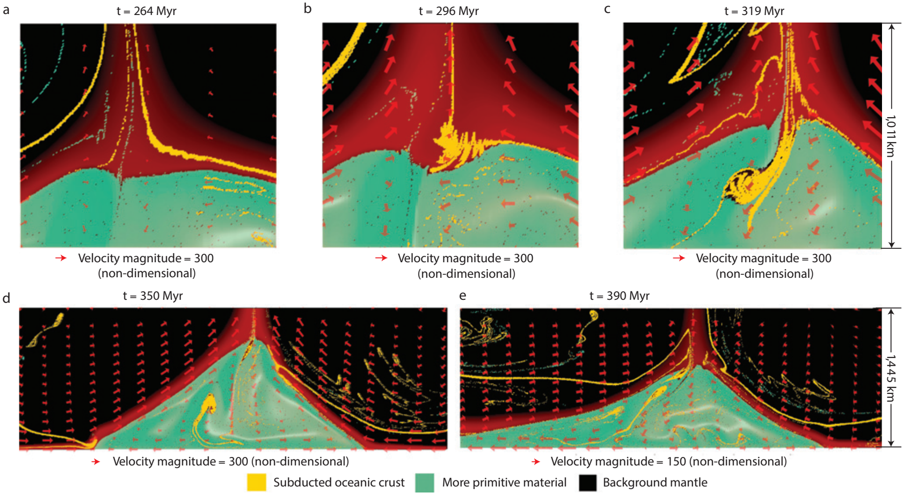

(Li, McNamara, Garnero, Nat. Geosc. 2014)

Effect of numerical resolution
Li and McNamara (2013)

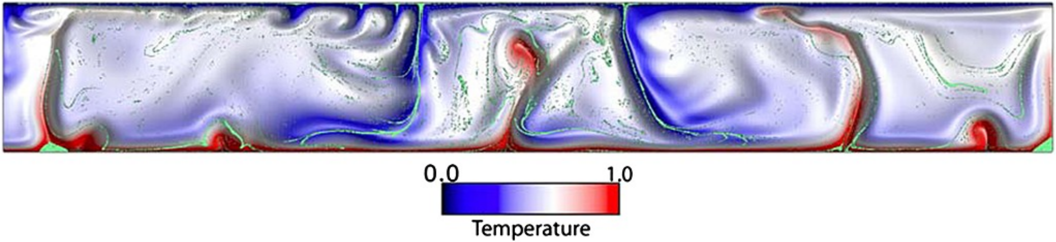

- Most models have a thick crust because of resolution issues.
- High resolution calculations show that a 6km thick crust is more difficult to segregate.
- Segregation can be helped by the presence of weak post-perovskite (Nakagawa & Tackley, 2013).

The fate of the subducted crust

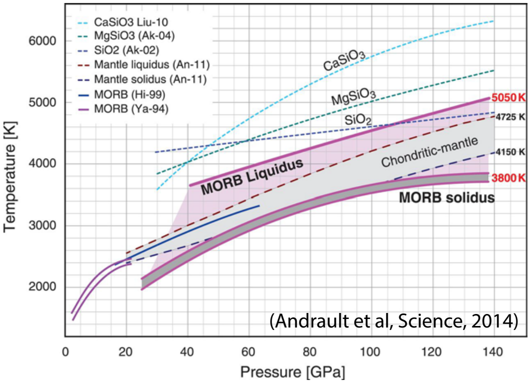

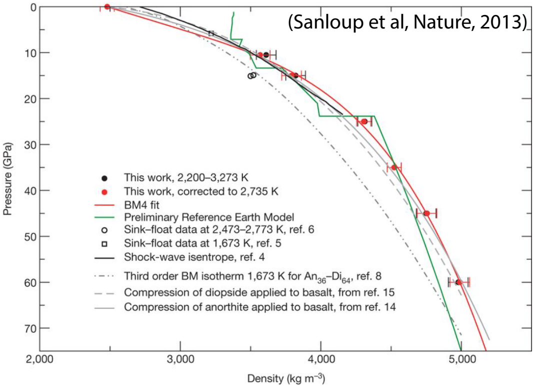

- MORBs likely melt on their way down (Andrault et al., 2014).
- Their density as liquid should make them negatively buoyant and join the ULVZs (Sanloup et al., 2013).

Outline

Entrainment with time
Le Bars and Davaille (2004)

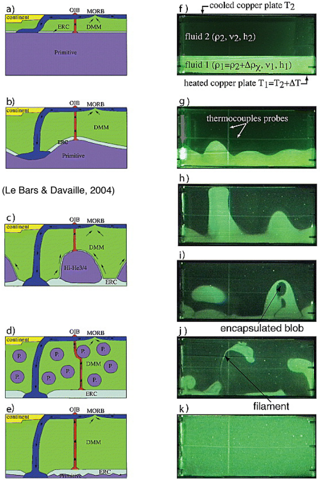

- Gradual entrainment at the interface of a layered system makes it undergo regime transitions.
- Doming regime (Davaille, 1999) could explain the anomalous topography of the Pacific superswell and south Africa.
- An intrinsically denser material can become temporally less dense because of high temperature and rise $\Rightarrow$ compatible with LLSVPs less dense than normal mantle (Koelemeijer et al., 2017).
- What could be the origin of the initial layering?

Outline

Thermal effect of continents

- Old continents (cratons) are parts of the surface that are not recycled back in the mantle and resist deformation.
- The question of the formation and stability of continents in a convective mantle has not yet been fully solved.
- Heat transfer across cratons happens by diffusion: less efficient than lithosphere recycling.
- The continuity of both temperature and heat flux at the boundary between the continental lithosphere and the less viscous underlying mantle can be modelled as a Robin boundary condition with a small Biot number (Grigné et al., 2007a,b; Guillou and Jaupart, 1995).

$\Rightarrow$ Small heat flux out of the convective mantle.

$\Rightarrow$ the mantle underneath heats up, which focuses upwelling plumes, which pushes the continent away (Gurnis, 1988).

Effects of a fixed continent
(Grigné et al., 2007a,b; Guillou and Jaupart, 1995)

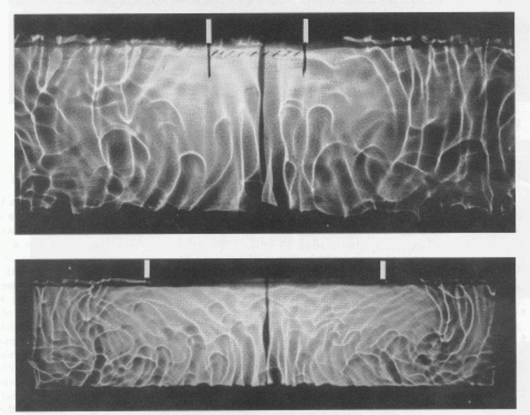

(Guillou & Jaupart, 1995)

- Experiment: no–slip BCs.
- Numerical model: free–slip BCs, even below the continent.
- High $Ra \Rightarrow$ Many plumes that get organised in a large scale circulation.

Motion of a small continent
Grigné, PhD thesis, 2003

- Cycles similar to that described by Gurnis (1988):
- Insulating effect $\Rightarrow$ focuses hot plumes $\Rightarrow$ the continent is pushed away.
- Small continent: the insulating effect is modest, the continent gets stuck above downwelling currents before new upwellings can develop and push the continent.
- The direction of the continent is randomised at each cycle.

$\Rightarrow$ erratic motion!

Motion of a large continent

Grigné, PhD thesis, 2003

- Once the continent starts to move, it keeps being attracted by a downwelling current at its leading edge while being pushed at its trailing side by upwelling currents it generates.
- For intermediate sizes, the reversals are still possible.

Motion of the continent as function of it size

Grigné, PhD thesis, 2003

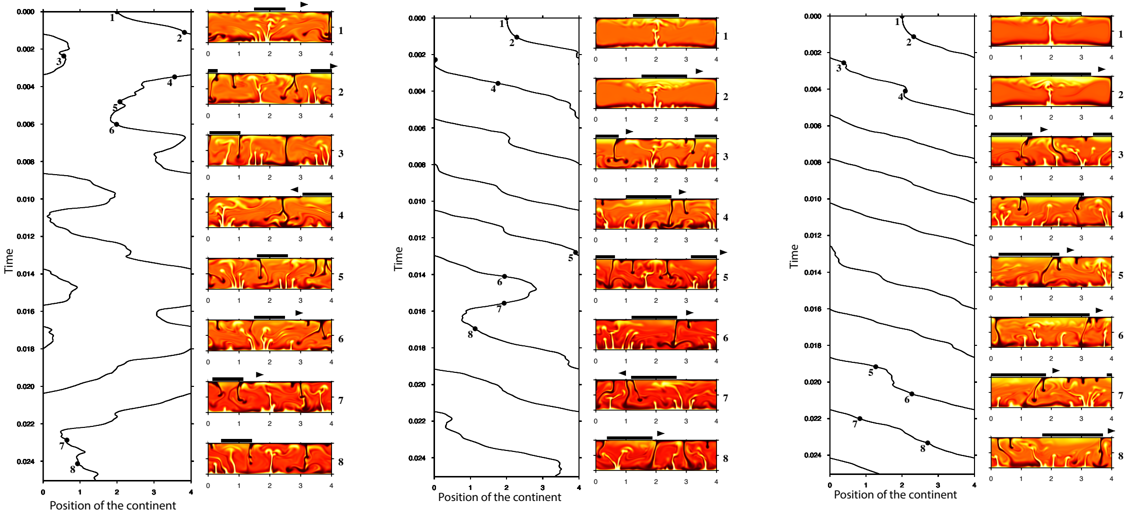

Effects of continents on a spherical 3D Earth

- 3D: continents can also rotate.
- Plate tectonics: Interaction between oceanic and continental plates of various rigidity is much more complex.

Distribution of seafloor ages
Cogné and Humler (2004)

- Thermal convection: down-welling current initiated when the boundary layer has cooled enough.
- Plate tectonics: subduction of plates of any age!

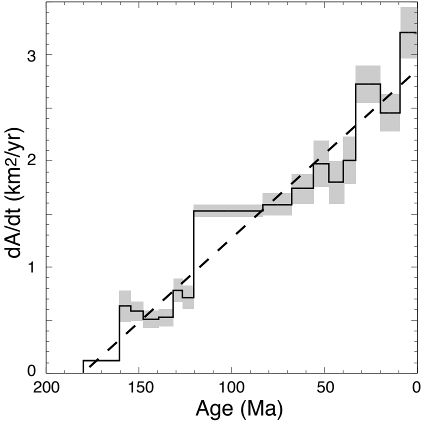

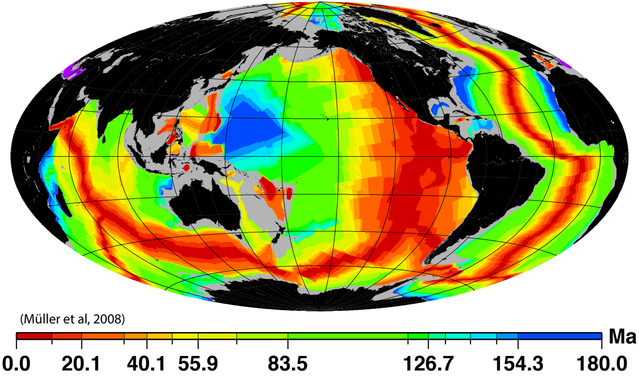

Mixed heating convection

Labrosse and Jaupart (2007)

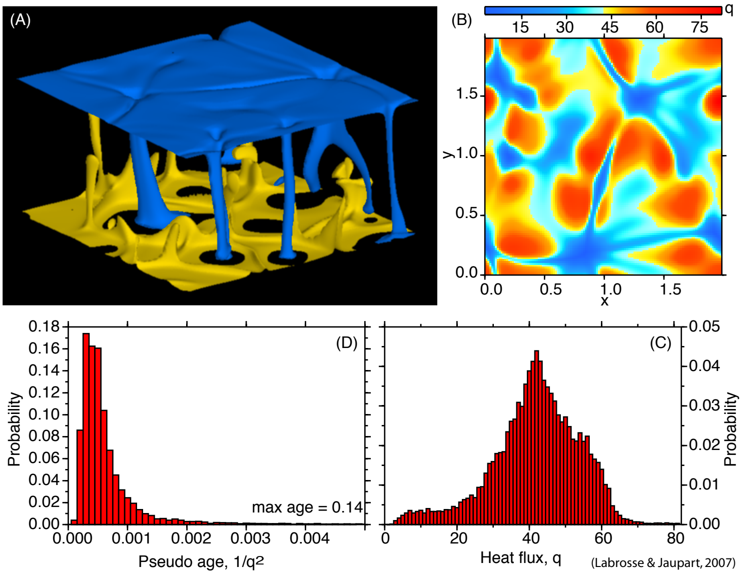

(Labrosse & Jaupart, 2007)

Convection with pseudo-plastic yielding
Labrosse and Jaupart (2007)

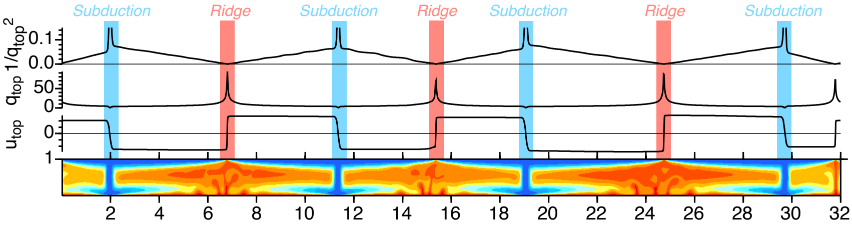

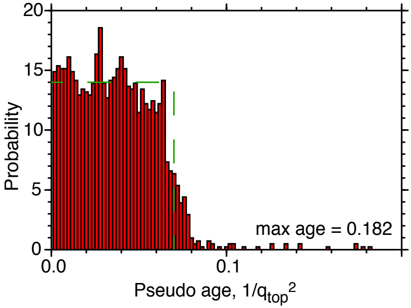

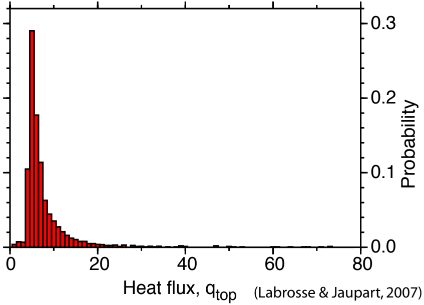

(Labrosse & Jaupart, 2007)

Possible explanation?
Labrosse and Jaupart (2007)

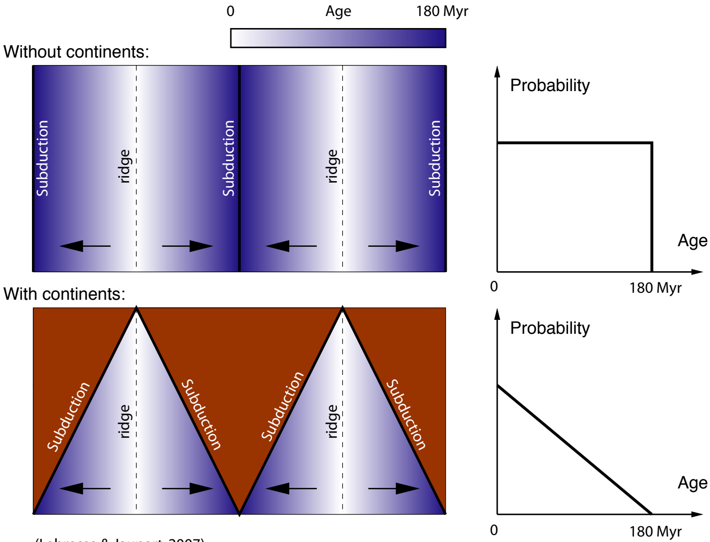

(Labrosse & Jaupart, 2007)

Test in a self-consistent model
Coltice et al. (2012)

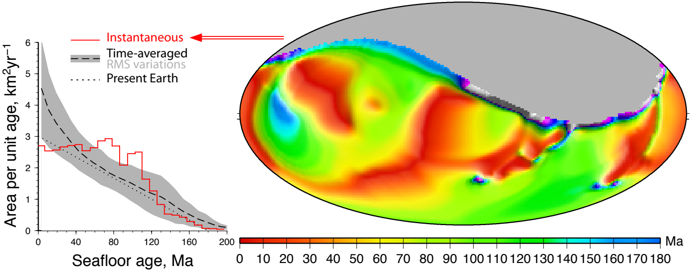

(Coltice et al, Science, 2012)

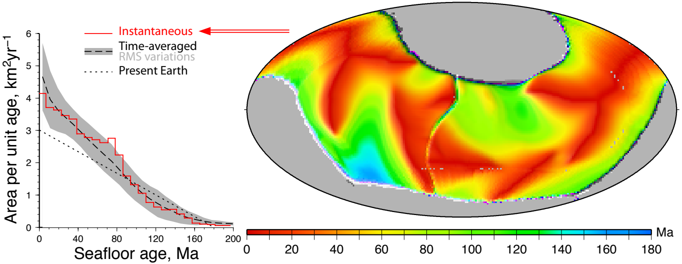

(Coltice et al, Science, 2012)

Part III

Application to the thermal evolution of the Earth

Principle for thermal evolution models

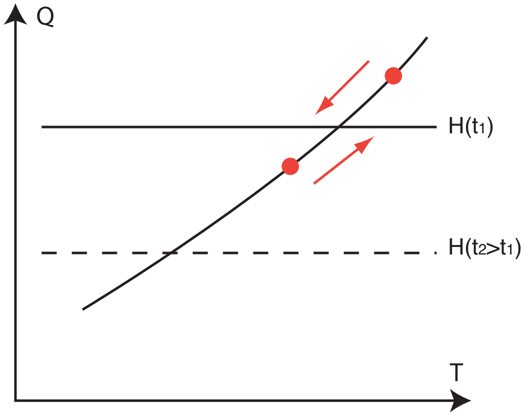

- Global energy balance

$$MC_P \frac{dT}{dt} = -Q(T) + H(t)$$

- Evolution time scale

$$\tau = \frac{MC_P T}{Q(T)}$$

- The Urey number (time dependent)

$$Ur = 100 \frac{H}{Q}$$

- Question:
  - what is the function $Q(T)$ for mantle convection?

Boundary layer scaling for thermal evolution model

- Boundary layer scaling

$$\Rightarrow q = C\frac{k\Delta T}{d} \mathit{Ra}^{1/3}\left(\frac{T_i}{\Delta T}\right)^{4/3}$$

- Assuming the scaling applies to mantle convection, hence to the present time $(t = 0)$: Q_0, T_0.
- Scaling of surface heat flow:

$$Q(T) = Q_0\left(\frac{T}{T_0}\right)^{4/3}\left(\frac{\eta(T)}{\eta_0}\right)^{-1/3}$$

- Given the present Urey number: $Ur = 100H/Q \in [20-50]$.
- Solve the energy equation backward from the present time:

$$MC\frac{dT}{dt} = H(t) - Q(T)$$

The low Urey number "paradox"

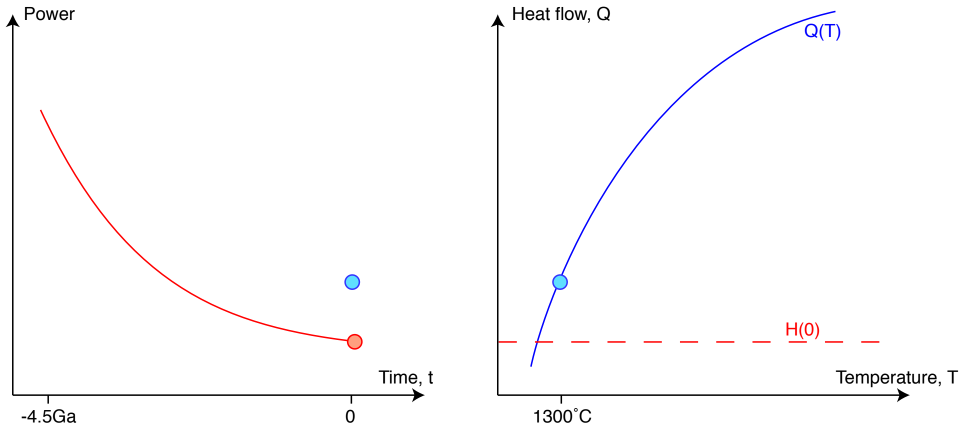

$$MC\frac{dT}{dt} = H(t) - Q(T); \qquad Q(T) = Q_0 \left(\frac{T}{T_0}\right)^{4/3} \left(\frac{\eta(T)}{\eta_0}\right)^{-1/3}$$

Urey number: $Ur = 100H/Q$

The low Urey number "paradox"

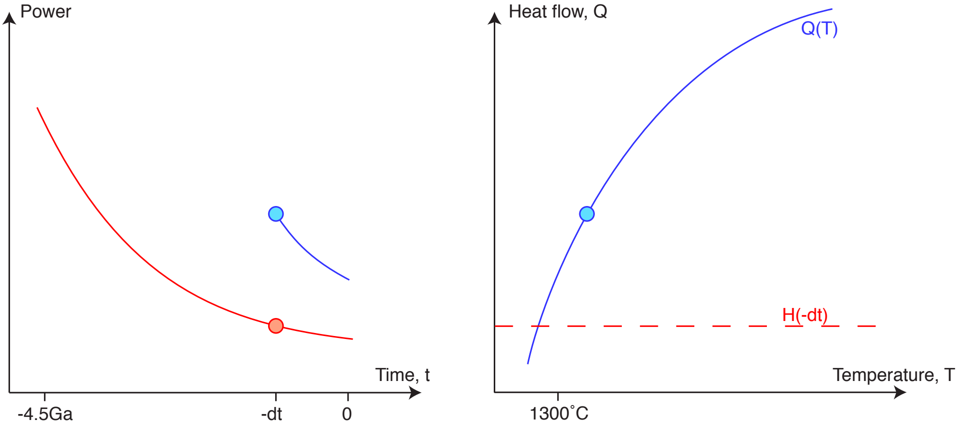

$$MC\frac{dT}{dt} = H(t) - Q(T); \qquad Q(T) = Q_0\left(\frac{T}{T_0}\right)^{4/3}\left(\frac{\eta(T)}{\eta_0}\right)^{-1/3}$$

Urey number: $Ur = 100H/Q$

The low Urey number "paradox"

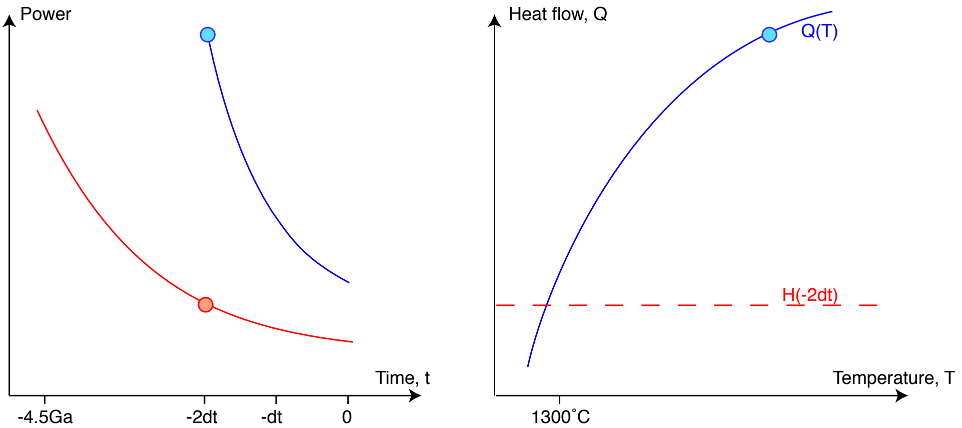

$$MC\frac{dT}{dt} = H(t) - Q(T); \qquad Q(T) = Q_0 \left(\frac{T}{T_0}\right)^{4/3} \left(\frac{\eta(T)}{\eta_0}\right)^{-1/3}$$

Urey number: $Ur = 100H/Q$

Feedback with temperature-dependent viscosity

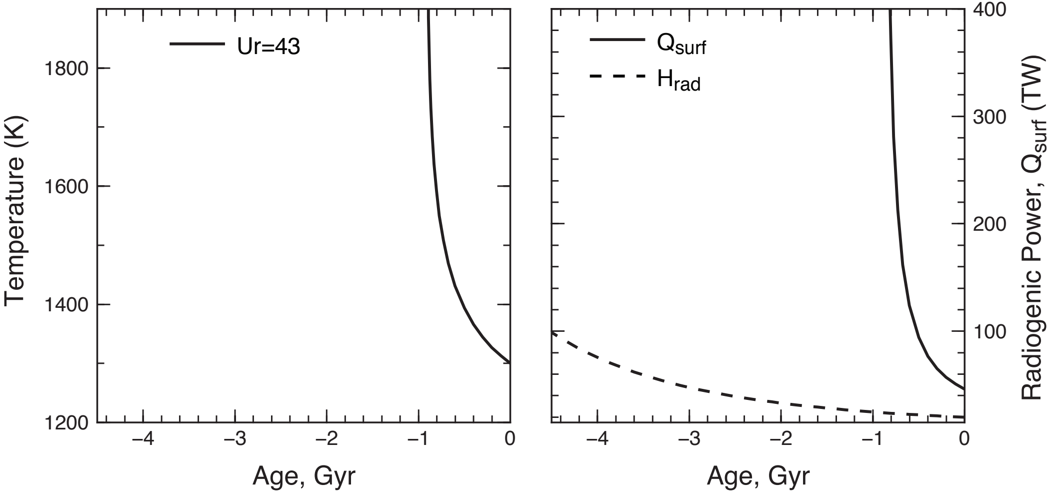

Feedback with temperature-dependent viscosity

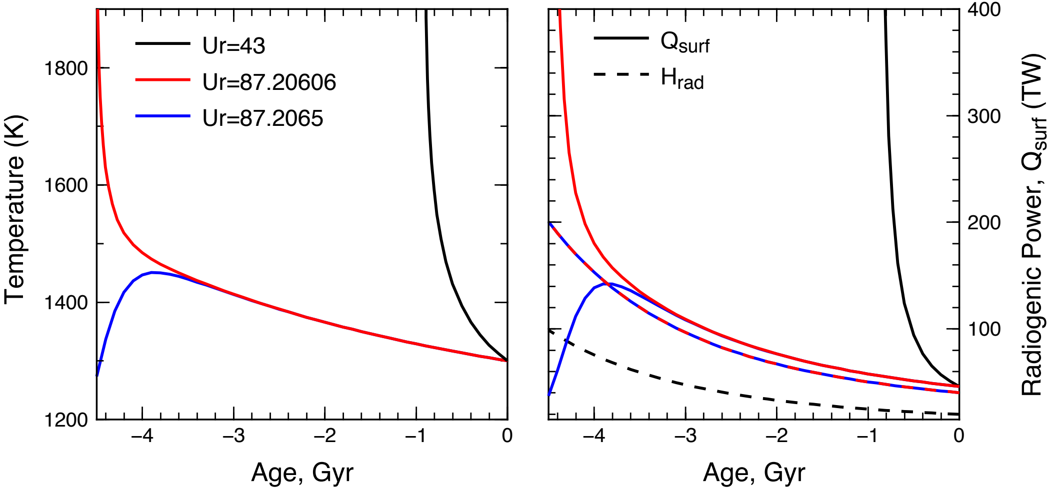

Proposed solutions

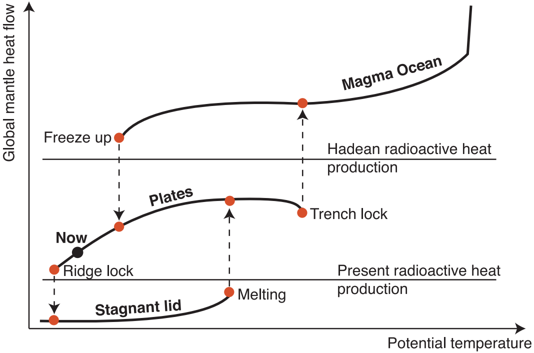

(adapted from Sleep, 2000)

- Convection in planetary mantle may have existed in several regimes.
- Layered mantle convection $\Longrightarrow$ lower cooling efficiency (McKenzie and Richter, 1981). But the inferred lower mantle temperature is too large to keep it solid (Schubert and Spohn, 1981).
- A smaller exponent β in the $q = ARa^{\beta}$ scaling law (Christensen, 1985; Conrad & Hager, 1999; Sleep, 2000; Korenaga, 2003).
- Differential core-mantle cooling (another type of layered model).

Proposed solutions

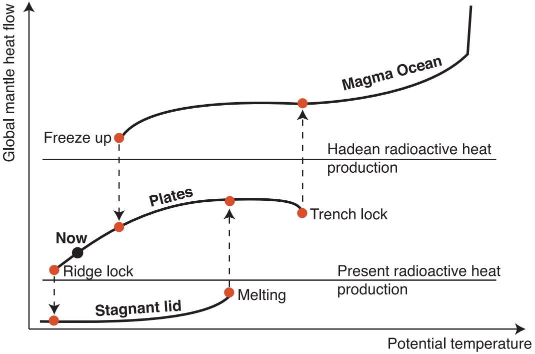

(adapted from Sleep, 2000)

- Convection in planetary mantle may have existed in several regimes.
- Layered mantle convection $\Longrightarrow$ lower cooling efficiency (McKenzie and Richter, 1981). But the inferred lower mantle temperature is too large to keep it solid (Schubert and Spohn, 1981).
- A smaller exponent β in the $q = ARa^{\beta}$ scaling law (Christensen, 1985; Conrad & Hager, 1999; Sleep, 2000; Korenaga, 2003).
- Differential core-mantle cooling (another type of layered model).

Proposed solutions

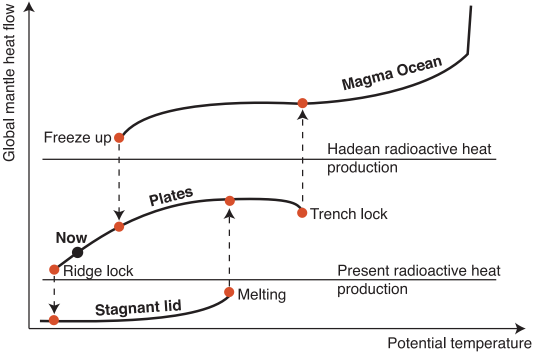

(adapted from Sleep, 2000)

- Convection in planetary mantle may have existed in several regimes.
- Layered mantle convection $\Longrightarrow$ lower cooling efficiency (McKenzie and Richter, 1981). But the inferred lower mantle temperature is too large to keep it solid (Schubert and Spohn, 1981).
- A smaller exponent β in the $q = ARa^{\beta}$ scaling law (Christensen, 1985; Conrad & Hager, 1999; Sleep, 2000; Korenaga, 2003).
- Differential core-mantle cooling (another type of layered model).

Proposed solutions

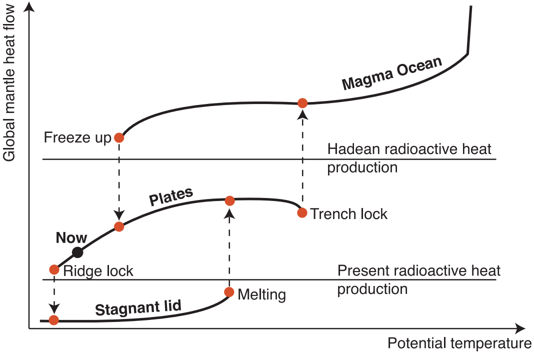

(adapted from Sleep, 2000)

- Convection in planetary mantle may have existed in several regimes.
- Layered mantle convection $\Longrightarrow$ lower cooling efficiency (McKenzie and Richter, 1981). But the inferred lower mantle temperature is too large to keep it solid (Schubert and Spohn, 1981).
- A smaller exponent β in the $q = ARa^{\beta}$ scaling law (Christensen, 1985; Conrad & Hager, 1999; Sleep, 2000; Korenaga, 2003).
- Differential core-mantle cooling (another type of layered model).

A lower β exponent to decrease the feedback?

Christensen (1985):

> local resisting forces in the subduction region. The cause for this resistance may be (1) shear on the thrust fault toward the overriding plate, (2) resistance against the bending of the downgoing plate, (3) resistance against penetration into a high viscosity layer at greater depth, (4) resistance against bending or viscous deformation at the boundary between upper and lower mantle, or (5) resistance against penetration through an endothermic phase boundary [*Christensen and Yuen*, 1984]. In cases 1, 2, and 5 the resisting force would be entirely independent from the asthenospheric temperature and viscosity, possibly also in case 4. The compressive stress which is usually

$\Rightarrow$ A decreased feedback between the mantle temperature and the surface heat flow.

Effect of the β exponent on thermal evolution

$$Q(T) = Q_0 \left(\frac{T}{T_0}\right)^{1+\beta} \left(\frac{\eta(T)}{\eta_0}\right)^{-\beta}$$

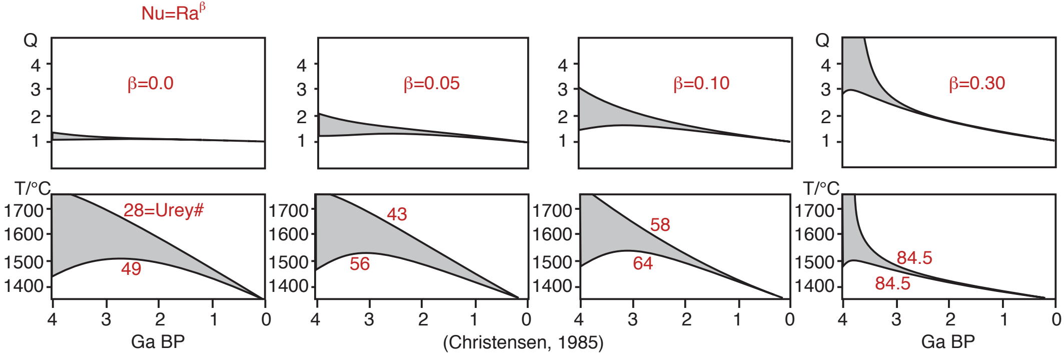

Same solution was advocated by Conrad & Hager (1999, 2001), Sleep (2000), Korenaga (2003).

Problem: No self-consistent dynamical model gives such low values of β

Effect of the β exponent on thermal evolution

$$Q(T) = Q_0 \left(\frac{T}{T_0}\right)^{1+\beta} \left(\frac{\eta(T)}{\eta_0}\right)^{-\beta}$$

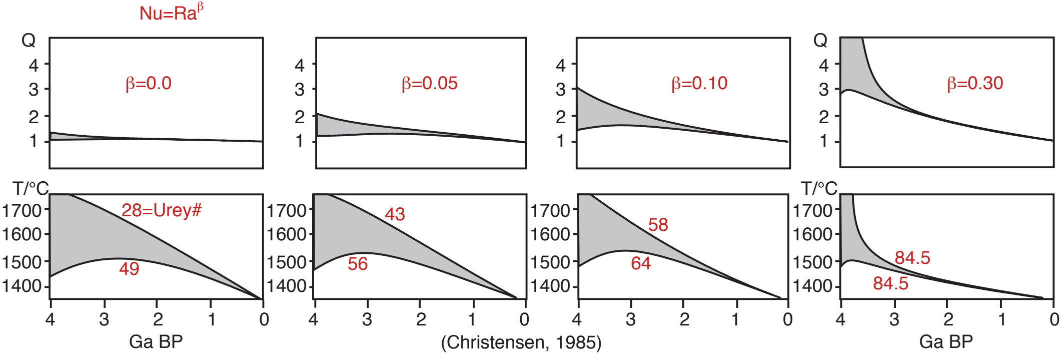

Same solution was advocated by Conrad & Hager (1999, 2001), Sleep (2000), Korenaga (2003).
Problem: No self-consistent dynamical model gives such low values of β

Alternative scenario

- Standard approach:

$$MC\frac{dT}{dt} = H(t) - Q(T)$$

parameterised by the mantle potential temperature only.

$\Rightarrow$ Core and mantle assumed to cool at the same pace.

- Assume instead that the core is cooling and not the mantle:

$\Rightarrow$ No feedback from temperature dependence of the mantle viscosity!

$$M_M C_M \frac{dT_M}{dt} = H(t) - Q(T_M) + Q_{CMB}$$

$$M_C C_C \frac{dT_C}{dt} = -Q_{CMB}$$

- Standard approach:

$$MC\frac{dT}{dt} = H(t) - Q(T)$$

parameterised by the mantle potential temperature only.

$\Rightarrow$ Core and mantle assumed to cool at the same pace.

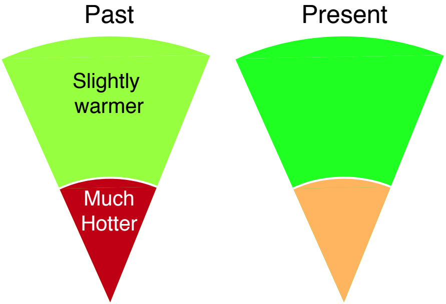

- Assume instead that the core is cooling and not the mantle:

$\Rightarrow$ No feedback from temperature dependence of the mantle viscosity!

$$M_M C_M \frac{dT_M}{dt} = H(t) - Q(T_M) + Q_{CMB}$$

$$M_C C_C \frac{dT_C}{dt} = -Q_{CMB}$$

A modified Urey number

Labrosse, in AGU Mon. 207, 2016

- Core heat flow is a heat source to the mantle. Assume $Q_{CMB} = 16\,\mathrm{TW}$.

⇒ Modified Urey number:

$$Ur^{\star} = \frac{H + Q_{CMB}}{Q_{surface}} \geq 0.78$$

- How can we constrain the CMB heat flow?

Evidences for the core cooling faster than the mantle

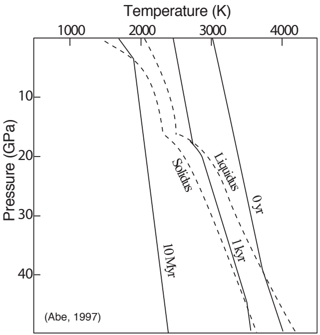

- Total mantle cooling in 4.5 Gyr constrained by the phase diagram of the upper mantle: $\Delta T_m < 200K$

- Core heat flow $> 10\mathrm{TW}$ constrained by
  - thermodynamics of the geodynamo with a large thermal conductivity ($> 90\mathrm{W/m/K}$).
  - double crossing of the Pv$\rightarrow$PPv phase boundary.

$\Rightarrow$ $\Delta T_c > 750\mathrm{K}$

Evidences for the core cooling faster than the mantle

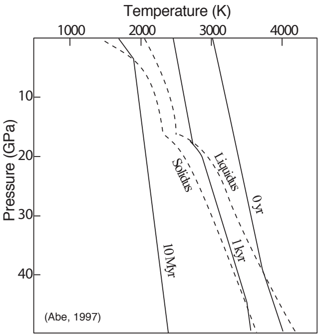

- Total mantle cooling in 4.5 Gyr constrained by the phase diagram of the upper mantle: $\Delta T_m < 200K$

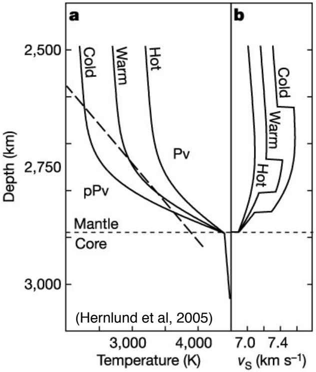

- Core heat flow $> 10\text{TW}$ constrained by
  - thermodynamics of the geodynamo with a large thermal conductivity ($> 90\text{W/m/K}$).
  - double crossing of the Pv→PPv phase boundary.

$\Rightarrow \Delta T_c > 750\text{K}$

Dense partial melt pocket at the base of the mantle

- Large V_S anomalies in the lower mantle $\rightarrow$ thermal and chemical heterogeneity.
- ULVZs at the edges of dense thermo-chemical piles. Interpreted as pockets of dense partial melt.

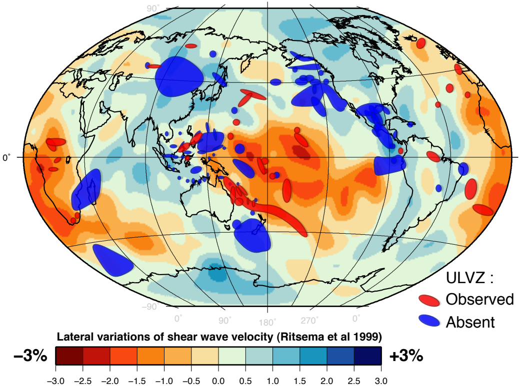

(Adapted from McNamara et al, 2010)

- If there is melt now at the bottom of the mantle, there must have been more in the past!

Crystallisation of a basal magma ocean (BMO)
Labrosse et al. (2007)

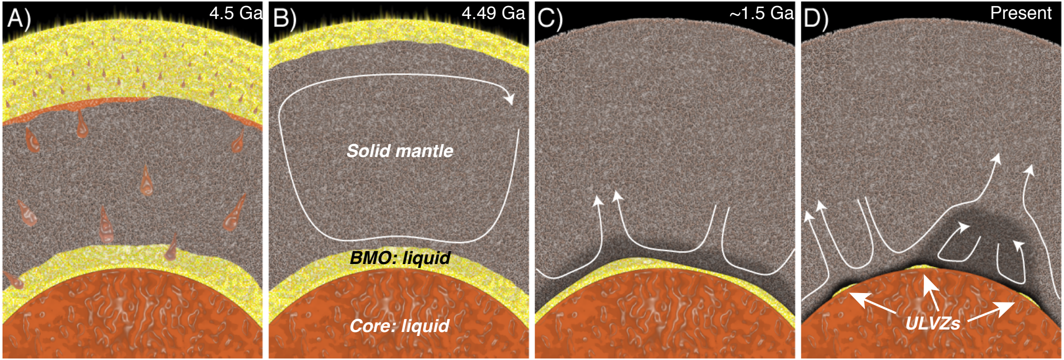

(Labrosse, Hernlund, Coltice, 2007)

- ULVZ: Dense partial melt at present
- Cooling of the core evidenced by the maintenance of the geodynamo for at least 3.5 Gyrs.
- $\Rightarrow$ More melt in the past!
- Fractional crystallisation $\Rightarrow$ compositional variations.

Time necessary for the crystallisation of the basal magma ocean

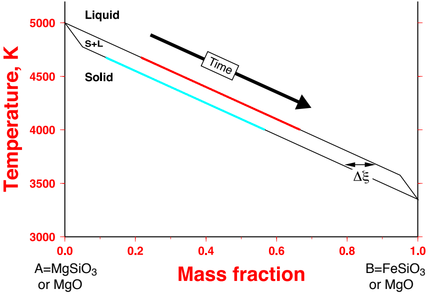

$$\tau = \frac{MC\Delta T}{Q} \sim 6\mathrm{Gyr}$$

$$M = 2\ 10^{24}\mathrm{kg},\ \ C \sim 1000\mathrm{JK^{-1}kg^{-1}}$$
$$\Delta T \sim 1000\mathrm{K},\ \ Q \sim 10\mathrm{TW}.$$

Time scale controlled by

- the heat flux taken up by convection in the solid mantle,
- the variation of the liquidus with chemical composition,
- the heat capacity of the core.

Going beyond the cartoon requires to understand the effects of the solid–liquid phase change on mantle convection.

Andrault, D., G. Pesce, M. A. Bouhifd, N. Bolfan-Casanova, J.-M. Hénot, and M. Mezouar (2014). Melting of subducted basalt at the core-mantle boundary. *Science* **344**: 892–895.

Becker, T. W. and L. Boschi (2002). A comparison of tomographic and geodynamic mantle models. *Geochem. Geophys. Geosyst.* **3**:

Bercovici, D. and S.-i. Karato (2003). Whole-mantle convection and the transition–zone water filter. *Nature* **425**: 39–44.

Bercovici, D. and Y. R. Ricard (2014). Plate tectonics, damage and inheritance. *Nature* **508**: 513–516.

Carlson, R. L. and H. P. Johnson (1994). on modeling the thermal evolution of the oceanic upper-mantle: an assessment of the cooling plate model on modeling the thermal evolution of the oceanic upper-mantle: an assessment of the cooling plate model. *J. Geophys. Res.* **99**: 3201–3214.

Christensen, U. R. and A. W. Hofmann (1994). Segregation of subducted oceanic crust in the convecting mantle. *J. Geophys. Res.* **99**: 19867–19884.

Cogné, J.-P. and E. Humler (2004). Temporal variation of oceanic spreading and crustal production rates during the last 180 My. *Earth Planet. Sci. Lett.* **227**: (3-4), 427–439.

Coltice, N., T. Rolf, P. J. Tackley, and S. Labrosse (2012). Dynamic Causes of the Relation Between Area and Age of the Ocean Floor. *Science* **336**: 335–338.

- Curbelo, J., L. Duarte, T. Alboussière, F. Dubuffet, S. Labrosse, and Y. Ricard (2019). Numerical solutions of compressible convection with an infinite Prandtl number: comparison of the anelastic and anelastic liquid models with the exact equations Compressible convection with infinite Prandtl number. *J. Fluid Mech* **873**: 646–687.
- Davaille, A. and C. Jaupart (1993). Transient high-Rayleigh-number thermal convection with large viscosity variations. *J. Fluid Mech.* **253**: 141–166.
- Davaille, A. and C. Jaupart (1994). Onset of thermal convection in fluids with temperature-dependent viscosity: Application to the oceanic mantle. *J. Geophys. Res.* **99**: 19853–19866.
- Davaille, A. (1999). Simultaneous Generation of Hotspots and Superswells by Convection in a Heterogeneous Planetary Mantle. *Nature* **402**: 756–760.
- Davis, E. E., D. S. Chapman, K. Wand, H. Villinger, A. T. Fisher, S. W. Robinson, J. Grigel, D. Pribnow, J. Stein, and K. Becker (1999). Regional heat flow variations across the sedimented Juan de Fuca ridge eastern flank: constraints on lithospheric cooling and lateral hydrothermal heat transport. *J. Geophys. Res.* **104**: 17, 675–17, 688.
- Dumoulin, C., D. Bercovici, and P. Wessel (1998). A continuous plate tectonic model using geophysical data to estimate plate-margin widths, with a seismicity-based example. *Geophys. J. Int.* **133**: 379–389.

- Grigné, C., S. Labrosse, and P. J. Tackley (2005). Convective heat transfer as a function of wavelength: Implications for the cooling of the Earth. *J. Geophys. Res.* **110**: doi:10.1029/2004JB003376, B03409.
- Grigné, C., S. Labrosse, and P. J. Tackley (2007a). Convection under a lid of finite conductivity in wide aspect ratio models: effect of continents on the wavelength of mantle flow. *J. Geophys. Res.* **112**: B08403.
- Grigné, C., S. Labrosse, and P. J. Tackley (2007b). Convection under a lid of finite conductivity: Heat flux scaling and application to continents. *J. Geophys. Res.* **112**: B08402.
- Guillou, L. and C. Jaupart (1995). On the effect of continents on mantle convection. *J. Geophys. Res.* **100**: 24217–24238.
- Gurnis, M. (1988). Large-Scale Mantle Convection and the Aggregation and Dispersal of Supercontinents. *Nature* **332**: 695–699.
- Jaupart, C., S. Labrosse, F. Lucazeau, and J.-C. Mareschal (2015). "7.06 - Temperatures, Heat, and Energy in the Mantle of the Earth". *Treatise on Geophysics (Second Edition)*. Ed. by G. Schubert. Second Edition. Oxford: Elsevier, 223–270.
- Jeffreys, H. (1930). The instability of a compressible fluid heated below. *Math. Proc. Camb. Phil. Soc.* **26**: 170–172.
- Kanda, R. V. and D. J. Stevenson (2006). Suction mechanism for iron entrainment into the lower mantle. *Geophys. Res. Lett.* **33**: 4–7.

Koelemeijer, P., A. Deuss, and J. Ritsema (2017). Density structure of Earth's lowermost mantle from Stoneley mode splitting observations. *Nature Communications* **8**: 1–10.

Krishnamurti, R. (1968). Finite Amplitude Convection With Changing Mean Temperature. Part 1. Theory. *J. Fluid Mech.* **33**: 445–455.

Labrosse, S., J. W. Hernlund, and N. Coltice (2007). A Crystallizing Dense Magma Ocean at the Base of Earth's Mantle. *Nature* **450**: 866–869.

Labrosse, S. and C. Jaupart (2007). Thermal Evolution of the Earth: Secular Changes and Fluctuations of Plate Characteristics. *Earth Planet. Sci. Lett.* **260**: 465–481.

Le Bars, M. and A. Davaille (2004). Whole layer convection in a heterogeneous planetary mantle. *J. Geophys. Res.* **109**: doi:10.1029/2003JB002617, B03403.

Leng, W. and S. Zhong (2008). Viscous heating, adiabatic heating and energetic consistency in compressible mantle convection. *Geophysical Journal International* **173**: 693–702.

Li, M. and A. K. McNamara (2013). The difficulty for subducted oceanic crust to accumulate at the Earth's core–mantle boundary. *J. Geophys. Res.* **118**: 1807–1816.

Li, M., A. K. McNamara, and E. J. Garnero (2014). Chemical complexity of hotspots caused by cycling oceanic crust through mantle reservoirs. *Nature Geoscience* **7**: 366–370.

- Lister, C. R. B., J. G. Sclater, E. E. Davis, H. Villinger, and S. Nagihara (1990). Heat flow maintained in ocean basins of great age: investigations in the north-equatorial West Pacific. *GJI* **102**: 603–628.
- McKenzie, D. P. and F. M. Richter (1981). parameterized thermal convection in a layered region and the thermal history of the Earth. *J. Geophys. Res.* **86**: 11667–11680.
- Moresi, L. N. and V. S. Solomatov (1995). Numerical investigation of 2D convection with extremely large viscosity variations. *Phys. Fluids* **7**: 2154–2162.
- Otsuka, K. and S. I. Karato (2012). Deep penetration of molten iron into the mantle caused by a morphological instability. *Nature* **492**: 243–246.
- Parmentier, E. M. and C. Sotin (2000). Three-dimensional numerical experiments on thermal convection in a very viscous fluid: Implications for the dynamics of a thermal boundary layer at high Rayleigh number. *Phys. Fluids* **12**: 609–617.
- Pouilloux, L., E. Kaminski, and S. Labrosse (2007). Anisotropic rheology of a cubic medium and implications for geological materials. *Geophysical Journal International* **170**: 876–885.
- Rayleigh, L. (1916). On convection currents in a horizontal layer of fluid, when the higher temperature is on the under side. *Phil. Mag.* **32**: 529–546.
- Ribe, N. M. (2018). *Theoretical mantle dynamics*. Cambridge University Press.

References VI

Ricard, Y., M. Richards, C. Lithgow-Bertelloni, and Y. LeStunff (1993). A Geodynamic Model Of Mantle Density Heterogeneity. *J. Geophys. Res.* **98**: 21895–21909.

Ritsema, J., H. J. v. Heijst, and J. H. Woodhouse (1999). Complex Shear Wave Velocity Structure Imaged Beneath Africa and Iceland. *Science* **286**: 1925–1928. eprint: `http://www.sciencemag.org/cgi/reprint/286/5446/1925.pdf`.

Sanloup, C., J. W. E. Drewitt, Z. Konôpková, P. Dalladay-Simpson, D. M. Morton, N. Rai, W. van Westrenen, and W. Morgenroth (2013). Structural change in molten basalt at deep mantle conditions. *Nature* **503**: 104–107.

Schubert, G. and T. Spohn (1981). Two–Layer Mantle Convection and the Depletion of Radioactive Elements in the Lower Mantle. *Geophys. Res. Lett.* **8**: 951–954.

Sleep, N. H. (2000). Evolution of the Mode of Convection within Terrestrial Planets. *J. Geophys. Res.* **105**: 17563–17578.

Smith, W. H. F. and D. T. Sandwell (1997). Global Sea Floor Topography from Satellite Altimetry and Ship Depth Soundings. *Science* **277**: 1956–1962. eprint: `http://science.sciencemag.org/content/277/5334/1956.full.pdf`.

Sotin, C. and S. Labrosse (1999). Three-dimensional Thermal convection of an isoviscous, infinite–Prandtl–number fluid heated from within and from below: applications to heat transfer in planetary mantles. *Phys. Earth Planet. Inter.* **112**: 171–190.

Tackley, P. J. (2000). Self-Consistent Generation of Tectonic Plates in Time-Dependent, Three-Dimensional Mantle Convection Simulations 1. Pseudoplastic yielding. *Geochem. Geophys. Geosyst.* **1**: 2000Gc000041.

White, D. B. (1988). The Planforms And Onset Of Convection With A Temperature-Dependent Viscosity. *J. Fluid Mech.* **191**: 247–286.